RSC Advances

PAPER

View Article Online
View Journal | View Issue

Open Access Article. Published on 10 August 2023. Downloaded on 11/6/2025 1:49:10 AM.
This article is licensed under a Creative Commons Attribution-NonCommercial 3.0 Unported Licence.

Check for updates

Cite this: *RSC Adv.*, 2023, **13**, 24003

Tail-approach based design, synthesis, and cytotoxic evaluation of novel disubstituted and trisubstituted 1,3-thiazole benzenesulfonamide derivatives with suggested carbonic anhydrase IX inhibition mechanism†

Samir Bondock, *[a] Tallah Albarqi,[a] Mohamed Abboud,[a] Tamer Nasr,[bc] Nada M. Mohamed [c] and Moaz M. Abdou [d]

A novel series of 2,4,5- and 2,3,4-trisubstituted thiazole hybrids with 1,3,4-thiadiazolylbenzenesulfonamide was designed following the tail approach as possible hCAIX inhibitors. The key intermediate **1** was condensed with thiosemicarbazide **2a** to give 1,3,4-thiadiazolylthiosemicarbazone **3**, which upon hetero-cyclization with substituted α-haloketones and esters afforded 2,4,5-trisubstituted thiazole-1,3,4-thiadiazole conjugates **4–8**. Furthermore, the trisubstituted thiazole-1,3,4-thiadiazole hybrids **12a–d** were synthesized *via* the regioselective cyclization of 4-substituted-1,3,4-thiadiazolylthiosemicarbazones with phenacyl bromide. The cyclized 2,4-disubstituted thiazole **4** enhanced cytotoxicity by nine, four and two times against HepG-2, Caco2, and MCF-7, respectively. Moreover, the simple methyl substitution on the thiosemicarbazone terminus **9a** improved the parent derivative **3** cytotoxicity by nine, fourteen, and six times against HepG-2, Caco2, and MCF-7, respectively. This astonishing cytotoxicity was elaborated with hCAIX molecular docking simulation of **4**, **9a**, and **12d** demonstrating binding to zinc and its catalytic His94. Furthermore, molecular dynamic simulation **9a** revealed stable hydrogen bonding with hCAIX with interaction energy of −61.07 kcal mol^{-1} and $\Delta G_{binding}$ MM-PBSA of −9.6 kcal mol^{-1}.

Received 17th April 2023
Accepted 3rd August 2023

DOI: 10.1039/d3ra02528d

rsc.li/rsc-advances

1. Introduction

There is a rising rate of research in medicinal chemistry to discover new effective and specific chemotherapeutic agents for cancer treatment.[1] Although many available anticancer drugs exist, drug resistance is still a major problem for their effective use. The hybridization approach is considered one of the most effective methods in drug design to attain novel anticancer agents capable of limiting their proliferation.[2] The synergistic effects of the hybrid structures can display pharmacological properties that are higher than those of individual structures, as well as decreased toxicity and fewer adverse effects. This trend in drug design is most obvious in thiazole chemistry,[3] where a growing number of novel thiazole-derived hybrids have been described with a strong emphasis on their various enzyme-inhibitory properties.[4] Among the several thiazole derivative platforms, promising and expanding applications with the sulfonamide system have been well exploited for producing carbonic anhydrase inhibitors.[5] Furthermore, sulfonamide-substituted 1,3,4-thiadiazoles have been demonstrated to have potential carbonic anhydrase inhibitory characteristics with anticancer activity.[6]

Carbonic anhydrases (hCAs, EC 4.2.1.1) are metalloenzymes that control the balance between carbon dioxide and bicarbonate ions through the adding-removing water mechanism. Their catalytic activity involved zinc(II) ions as a cofactor to regulate the cellular pH.[7,8] To date, fifteen human isoforms have been isolated; 12 of them are catalytic isoforms with a zinc-binding site.[9–11] Out of the 12 catalytic isoforms, the transmembrane hCAIX and hCAXII were strongly correlated with cancer progression, which assisted the cancerous cell in accommodating the hypoxia conditions promoting metastases.[12] They were considered an interesting target for new anticancer agents' development, especially with their established protein structures. Despite their variable tissue distribution, the hCA isoforms show high similarity in their protein

[a]Chemistry Department, Faculty of Science, King Khalid University, 9004 Abha, Saudi Arabia. E-mail: bondock@mans.edu.eg

[b]Pharmaceutical Chemistry Department, Faculty of Pharmacy, Helwan University, 11795 Helwan, Cairo, Egypt

[c]Pharmaceutical Chemistry Department, Faculty of Pharmacy, Modern University for Technology and Information, MTI, 12055 Cairo, Egypt

[d]Egyptian Petroleum Research Institute, Nasr City, 11727, Cairo, Egypt

† Electronic supplementary information (ESI) available. See DOI: https://doi.org/10.1039/d3ra02528d

© 2023 The Author(s). Published by the Royal Society of Chemistry

Open Access Article. Published on 10 August 2023. Downloaded on 11/6/2025 1:49:10 AM.
This article is licensed under a Creative Commons Attribution-NonCommercial 3.0 Unported Licence.

structure. The main chain structure of the tumor-associated hCAIX demonstrated RMSD 2.02, 2.05, and 1.87 Å with hCAI, hCAII, and hCAXII, respectively.[13] Moreover, hCAIX shared 83 conserved amino acids with the other tumor-associated isoform hCAXII while sharing 79 and 75 conserved residues with hCAI and hCAII, respectively.[13]

Among the hCAIX inhibitors, thiadiazole-benzenesulfonamide derivatives had established appreciated activity, with the sulfonamide moiety acting as the zinc-binding group (ZBG). For instance, acetazolamide **AAZ** and methazolamide **MAZ** are clinically proven non-selective hCA inhibitors with thiadiazole sulfonamide core that possess the common structural features of classical inhibitors (Fig. 1).[14,15] Merging the thiadiazole scaffold with the ZBG benzenesulfonamide was followed into **Ia** showed hCAXII Ki of 34.2 nM and **Ib** had hCAIX Ki of 86.4 nM.[16] Several thiazole benzenesulfonamides had established valued hCA inhibition, such as **II** with Ki 0.4 and 0.11 μM of isoforms hCAI and hCAII, respectively.[17] Similarly, the thiazole-benzenesulfonamide hybrids **IIIa–c** were reported with a potential inhibition of hCAIX, especially when increasing the lipophilicity of **IIIa**. This lipophilicity optimization improved their inhibitory potentials by three and 1.5 times against hCAIX and hCAXII, respectively, upon adding a phenyl **IIIb** or 4-chlorophenyl **IIIc** moieties to the C_4-thiazole ring (Fig. 1).[18]

On the other hand, several thiosemicarbazone derivatives were reported as hCA isoform inhibitors, such as **IV–V**, which showed hCAII IC_{50} of 26.9 and 0.13 μM, respectively.[19,20] Moreover, the aromatic linked thiosemicarbazone proved appreciated inhibition against both hCA isoforms hCAI and hCAII with sub-micromolar IC_{50} values, including **VIa** and **VIb** with IC_{50} range 0.19–0.28 μM (Fig. 1).[21] Similarly, the naphthalene–thiosemicarbazone **VIIa** and **VIIb** hybrids were reported to exhibit hCAII inhibition at the micromolar level (Fig. 1), with their molecular docking simulation highlighting the importance of the thiosemicarbazone sulfur and nitrogen groups to anchor zinc ion and the binding site residues Gln91, Thr198, and Thr199.[20]

Based on the information above, we designed novel hCAIX inhibitors by optimizing the structure of the non-selective hCA inhibitor **AAZ** (Fig. 2). In the target compounds, we kept the sulfonamide moiety as a zinc-binding group. Besides its ability to bind to the zinc in the active site, the sulfonamide moiety could bind to His94, Leu198, and/or Thr199 through H-bond formation. We then replaced the 1,3,4-thiadiazole spacer of **AAZ** with 5-imino-4,5-dihydro-4-(phenyl)-1,3,4-thiadiazole moiety. The main reason is the ability of the imino group at C_5-thiadiazole to form a hydrogen bond with His64. It was proved that the role of His64 is shuttling the proton during hCAs catalytic activity.[13]

Moreover, the phenyl thiadiazole could form hydrophobic interactions with the amino acids within the active site of hCA, such as Leu198 and Leu135. Also, we replaced the small acetyl tail of **AAZ** with longer and flexible substituted thiosemicarbazide moieties. This moiety allows hydrogen bond formation with the amino acids Gln67, Asn62, Arg60, and/or Gln92 of the active site of hCA. On the other hand, the ring closure strategy was applied to introduce the thiazole moiety in the tail part by cyclization of the thiosemicarbazide moiety. Aromatic substitution at C_4 of the thiazole ring might form hydrophobic interaction with the Val131 or Leu91. Besides, the aromatic group at C_3-thiazole might form extra hydrophobic interaction with Gln92 and/or Val131. In a trial for finding the thiazole ring's best substitution pattern, we tried a set of

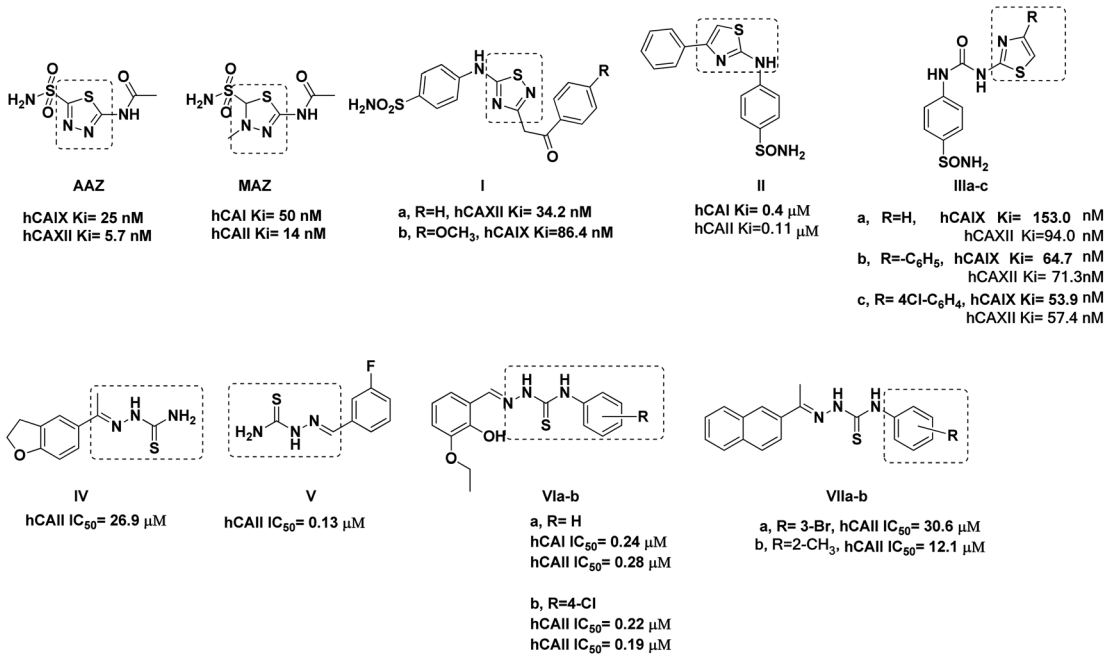

Fig. 1 Reported thiadiazole, thiazole, and thiosemicarbazone derivatives with carbonic anhydrase inhibition and anticancer activity.

 © 2023 The Author(s). Published by the Royal Society of Chemistry

Open Access Article. Published on 10 August 2023. Downloaded on 11/6/2025 1:49:10 AM.
This article is licensed under a Creative Commons Attribution-NonCommercial 3.0 Unported Licence.

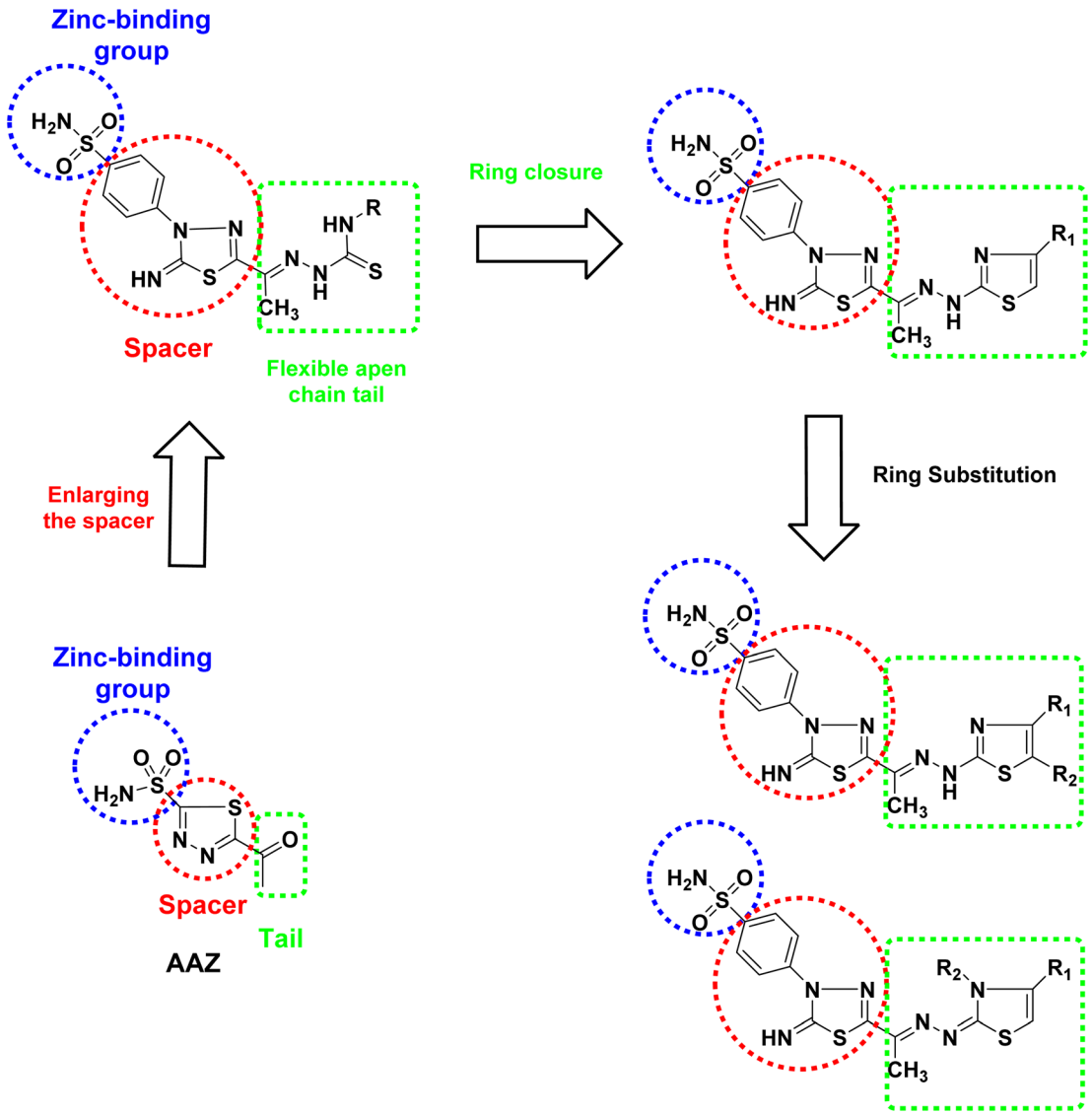

Fig. 2 Design the targeted 2,4,5- and 2,3,4-trisubstituted thiazole hybrids with 1,3,4-thiadiazolylbenzenesulfonaminde derivatives as hCAIX inhibitors.

substitutions to get 2,3,4- and 2,4,5-trisubstituted thiazole derivatives to adopt a conformation that might fill the unoccupied region of hCAIX active site.

2. Results and discussion

2.1. Chemistry

The synthetic strategy for constructing the target two series of disubstituted and trisubstituted 1,3-thiazole sulfonamide derivatives (Schemes 1 and 2).

2.1.1. Synthesis of 1,3,4-thiadiazolylbenzenesulfonaminde tagged with 2,4-disubstituted and 2,4,5-trisubstituted thiazole derivatives (4–8). Thiazole is easily obtainable *via* the Hantzsch reaction of α-haloketones with thiourea fragment.[22] In this context, the primary step for preparing novel functionalized 1,3-thiazole-based 1,3,4-thiadiazole is the reaction of 5-acetyl-3-*N*-(4-sulfamoylphenyl)-2-imino-1,3,4-thiadiazoline **1** with thiosemicarbazide **2a** followed by cyclization of product with sets of α-halocarbonyl reagents. Thus, treatment of **1** with thiosemicarbazide in boiling ethanol with a few drops of conc. HCl gave the corresponding condensation product **3** (Scheme 1). Spectral data and chemical transformation proved the structure of the later product. The IR spectrum of **3** revealed absorption bands at 3434–3151, 3141, 3102,1640, 1335, and 1248 cm^{-1} characteristic for $2NH_2$, 2NH, C=N, SO_2 groups, and C=S, respectively. Its ^{1}H-NMR spectrum exhibits the expected signals from aromatic protons and six singlet signals at δ 2.32, 7.39, 7.64, 8.60, 9.41, and 10.83 ppm assigned to CH_3, SO_2NH_2, ^{4}N–H^b, ^{4}N–H^a, NH and ^{2}N–H protons, respectively. The ^{13}C-NMR spectrum of **3** showed the existence of nine carbon signals which compatible with the suggested structure. The most significant carbon signals resonate at δ 12.50, 158.56, and 179.07 ppm, assignable to CH_3, thiadiazole-C_5, and C=S carbon, respectively. The mass spectrum (MS) of **3** revealed

Open Access Article. Published on 10 August 2023. Downloaded on 11/6/2025 1:49:10 AM.
This article is licensed under a Creative Commons Attribution-NonCommercial 3.0 Unported Licence.

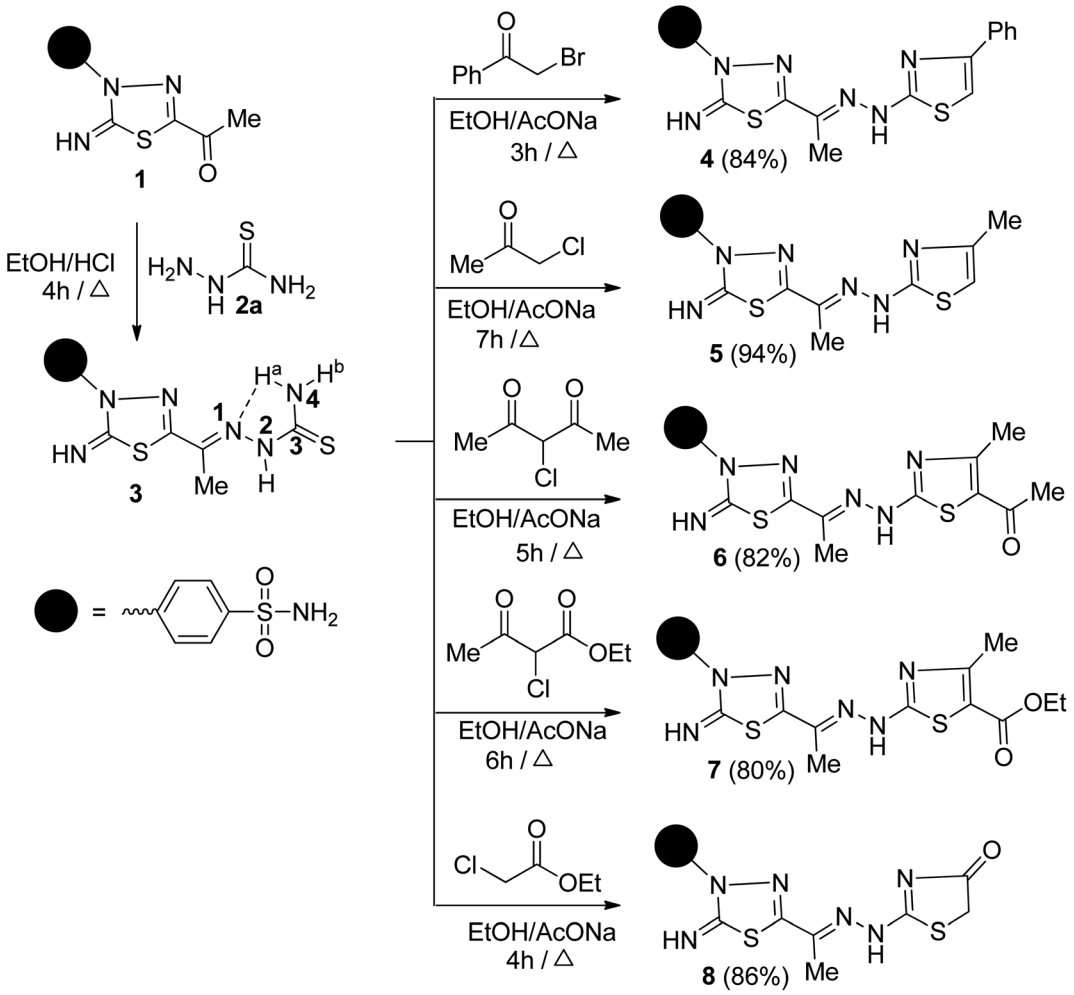

Scheme 1 Synthesis of 1,3,4-thiadiazolylbenzenesulfonaminde tagged with 2,4-disubstituted and 2,4,5-trisubstituted thiazole derivatives **4–8**.

a molecular ion peak (M^+) at $m/z = 371$ confirming its molecular weight.

It is worth mentioning that the ^4N-unsubstituted thiosemicarbazone **3** can adopt *syn* conformation (NHC=S) and 1*E* (C=N) configuration (Scheme 1) based on previous studies.[23] The suggested molecular configuration with the $^4N–H^b$ *cis* to the C=S group, leaving the second $^4N–H^a$ disposed of intramolecular H-bond formation with $^1N=C$. The proposed configuration of **3** supports the appearance of the germinal protons of the NH_2 group in the ^{1}H-NMR spectrum as magnetically nonequivalent protons.

Next, the reactivity of **3** with various α-chlorocarbonyl reagents was explored to prepare bioactive 1,3-thiazole-1,3,4-thiadiazole conjugates. Thus, the reaction of **3** with each of phenacyl bromide and chloroacetone in ethanol in the presence of sodium acetate under reflux afforded benzenesulfonamides **4** and **5**, respectively (Scheme 1). The structures of **4** and **5** were confirmed based on microanalyses and spectral data. For example, the IR spectrum of **5** displayed the lack of NH_2 and C=S functions and the presence of two bands at 3142, 3101 cm^{-1} for two NH groups besides the azomethine (C=N) band at 1602 cm^{-1}. The ^{1}H-NMR spectrum of **5** indicated six singlet signals at δ 2.13, 2.26, 6.30, 7.37, 9.29, and 11.79 ppm related to the two CH_3 groups, thiazole-H_5, NH_2, imine NH, and NH, as well as to the expected two doublets for the four aromatic protons. Its ^{13}C-NMR spectrum revealed two sp^3 hybridized carbon atoms at δ 13.34 and 17.46 ppm due to two methyl carbons, besides ten carbon signals assigned to sp^2 hybridized carbon atoms. The M^+ peaks at $m/z = 471$ and 409 in the mass spectra of **4** and **5** are compatible with their molecular formula ($C_{19}H_{17}N_7O_2S_3$) and ($C_{14}H_{15}N_7O_2S_3$), respectively.

Furthermore, the mass fragmentation pattern of **5** is depicted in Scheme S1.† Compound **5** underwent cleavage to give two ion peaks at $m/z = 128$ and 281 due to the formation of 2-methylamino-4-methylthiazole and 5-cyano-2-imino-3-(4-sulfamoylphenyl)-1,3,4-thiadiazoline, respectively. The formed thiazole cleavages further to produce the base peak at $m/z = 59$ (100%), which is assigned to 1,2-thiazine cation radical. On the other hand, the thiadiazole fragment cleavages further to give rise to a sulfanilamide ion peak at $m/z = 172$.

Similarly, 2,4,5-trisubstituted thiazoles **6** and **7** were obtained in good yields by heating **3** with each of 3-chloro-2,4-pentanedione and ethyl 2-chloroacetoacetate in ethanol in the presence of sodium acetate. Heterocyclization of **3** with ethyl

 © 2023 The Author(s). Published by the Royal Society of Chemistry

Open Access Article. Published on 10 August 2023. Downloaded on 11/6/2025 1:49:10 AM.
This article is licensed under a Creative Commons Attribution-NonCommercial 3.0 Unported Licence.

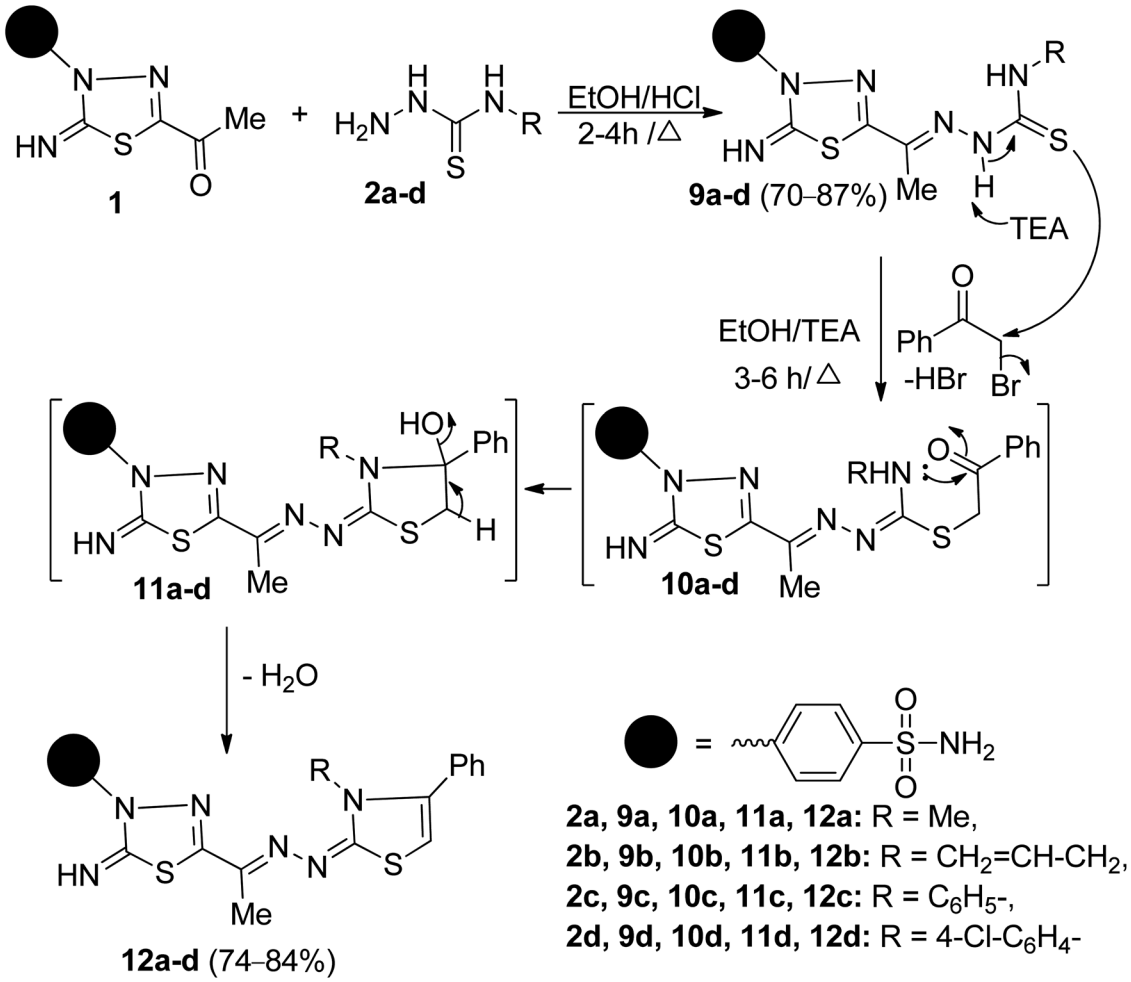

Scheme 2 Synthesis of 1,3,4-thiadiazolylbenzenesulfonaminde tagged with 2,3,4-trisubstituted thiazole derivatives **12a–d**.

chloroacetate in ethanol under reflux in sodium acetate furnished the thiazolidine-4-one **8** (Scheme 1). Their correct elemental analyses and spectral data clarified the structures of **6**, **7**, and **8**. Their IR spectra exhibited, in each case, a strong absorption band in the region 1713–1668 cm^{-1}, characteristic of the carbonyl function. The ^{1}H-NMR spectrum of **6**, as a representative example, showed, along with aromatic proton signals, six singlet signals, three signals exchangeable with D_2O, resonate downfield at δ 7.35, 9.25, 11.79 ppm corresponding to NH_2, and two NH protons, respectively, and three signals appeared upfield at δ 2.19, 2.26, 2.39 ppm related to three methyl protons. Its ^{13}C-NMR spectrum revealed the appearance of 14 carbon signals. The sp^3-hybridized carbon atoms resonated at δ 12.98, 27.48, 30.87 ppm is assignable to the three methyl carbons. Furthermore, the characteristic signal of the C=O resonates at δ 189.00 ppm. The mass spectrum of **6** showed a M^+ peak at m/z 451, which is adaptable to a molecular formula ($C_{16}H_{17}N_7O_3S_3$).

2.1.2. Synthesis of 1,3,4-thiadiazolylbenzenesulfonaminde tagged with 2,3,4-trisubstituted thiazole derivatives (12a–d). The cyclization reaction of 4-substituted thiosemicarbazones with α-haloketones represents the simple and convenient route to obtain 2,3,4-trisubstituted thiazoles.[24] we studied the site selectivity for the cyclization reaction of 4-substituted thiosemicarbazones with phenacyl bromide. Thus, condensation of 4-substituted thiosemicarbazide **2a–d**, obtained from treating substituted isothiocyanates with hydrazine hydrate in ethanol,[25,26] with 5-acetyl-1,3,4-thiadiazoline **1** in ethanol and the presence of HCl under reflux, afforded the corresponding compounds **9a–d** (Scheme 2).

The structures **9a–d** were proved based on their elemental analyses, spectral data, and chemical transformations. Their IR spectra exhibited characteristic absorption bands in the region 3339–3030 cm^{-1} attributed to NH_2 and three NH groups and at 1635–1625 cm^{-1} characteristics for conjugated azomethine (C=N) groups and 1247–1187 cm^{-1} due to thiocarbonyl groups, respectively. The mass spectra of **9a–d** exhibited a M^+ peak in each case, which was compatible with its molecular weight. The ^{1}H-NMR spectrum of **9a**, as an example of these series, revealed a doublet signal at δ 3.04 ppm due to methylamino protons, five singlet signals at δ 2.28, 7.66, 8.70, 11.04, and 11.43 ppm due to CH_3, NH_2, and three NH protons, respectively, and two doublet signals at δ 7.92 and 8.05 ppm due to four aromatic protons. Its ^{13}C-NMR spectrum exhibited 10 carbon signals. The sp^3

Open Access Article. Published on 10 August 2023. Downloaded on 11/6/2025 1:49:10 AM. This article is licensed under a Creative Commons Attribution-NonCommercial 3.0 Unported Licence.

hybridized carbon signals resonate at δ 12.78 and 31.53 ppm, attributed to two methyl carbons. The two downfield carbon signals appear at δ 167.79 and 178.67 ppm characteristics for C=NH and C=S, respectively. Hence, NMR spectra for these analogues, **9a–d**, showed only one set of peaks, demonstrating the *E* configuration's preferential formation. The $Z_{C=N}$ configuration is not observed because of steric hindrance, and the non-planar conformation of C=N–NH does not exist because it would violate the n–π conjugation.[27–29] To get more evidence on the geometry of our molecular structure, we performed Quantum DFT-B3LYP/6-31G(d) calculations for each isomer of **9a** as an example. Accordingly, the calculated energy for optimized geometry of the (*E*) isomer of −2194.475905 Hartree appears to be slightly lower than that of the (*Z*) isomer (−2194.465113 Hartree). Theoretically, the (*E*) isomer is more stable than the (*Z*) isomer, with an energy difference of 6.77 kcal mol^{-1} (ESI, Fig. S57†).

2,3,4-Trisubstituted thiazoles were prepared to investigate the effect of substituents inserted on the N-3 position for anticancer activity. Thus, cyclocondensation of **9a–d** with phenacyl bromide furnished a sole product, in each case, identified as 2,3,4-trisubstituted thiazoles **12a–d** (Scheme 2). Spectral data and microanalyses secured the structures of the later products. Their IR spectra were free of absorption bands in regions 3130–3100 cm^{-1} and 1247–1187 cm^{-1} related to two secondary NH groups and a thiocarbonyl group. For example, the ^{1}H-NMR spectrum of **12b** revealed four singlet signals at δ 2.27, 6.62, 7.46, 9.98 ppm due to CH_3, thiazole-H_5, NH_2, and NH protons, respectively, and a doublet signal resonates at δ 4.47 ppm due NCH_2 protons. It also exhibited two doublets of doublets, and one multiplet signal resonated around δ 5.12, 5.19, 5.82 ppm due to the vinyl protons (CH_2=CH), and two doublets resonate at δ 7.96 and 8.08 ppm, indicating the existence of 4-disubstituted benzene, besides the other expected signals for five aromatic ring residues. The ^{13}C-NMR spectrum of **12b** revealed eighteen carbon signals. The aliphatic carbons resonate at δ 12.49, 47.95 ppm, assignable for the carbons of CH_3, and NCH_2 groups, respectively. The olefinic carbons appear at δ 117.09, 132.07 ppm due to the carbons of the vinyl group (CH_2=CH). Further, the signals resonate at δ 102.35, 146.27, 155.51, 159.51, 171.48 ppm assignable to the carbons of thiazole-C_5, C=N, thiadiazole-C_5, thiazole-C_2, and thiadiazole-C_2, respectively. The mass spectrum showed a M^+ peak at m/z = 511, corresponding to a molecular formula $C_{22}H_{21}N_7O_2S_3$. The mass spectrometry fragmentations are characteristic of the appearance of the fragment at m/z = 496 and 470 due to the loss of methyl and allyl groups from the parent ion peak, respectively. The peak showed at m/z = 102 (59%), assigned to the loss of phenylacetylene molecule [M^+–C_8H_6] and the base peak appeared at m/z = 134 (100%) due to the formation of 2-phenylthirine cation radical $[C_8H_6S]^{+\cdot}$ that confirms the formation of thiazole ring.

The formation of **12a–d**, as depicted in Scheme 2, is expected to start with the S_N^2-displacement reaction of bromine atom by the thiolate anion of **9a–d**, generated from deprotonation of more acidic N–H^2 proton, to afford the non-isolable thioether intermediates **10a–d** that subsequently undergoes tandem 5-*exo-trig* ring closure *via* nucleophilic addition of a secondary NH group to C=O group to give intermediates **11a–d** that loss water molecule to afford the target compounds **12a–d**.Another structural feature of the synthesized thiazoles **12a–d** is they can theoretically exist in *EZ* or/and *EE* diastereomers. The preference formation of the thermodynamically stable diastereomers was demonstrated for **12a**-as example using B3LYP/6-31G(d) calculation. The results revealed that the optimized geometry for the diastereomer *EZ* has an energy of −2501.718252 Hartree, which is lower than that calculated for the *EE*-diastereomer (−2501.705865 Hartree) by about 7.77 kcal mol^{-1} (ESI, Fig. S58†).

2.2. Bio-evaluation

2.2.1. Cytotoxicity evaluation. The cytotoxicity potential of the synthesized derivatives **1**, **3–8**, **9a–d**, **12b**, and **12d** was evaluated *in vitro* against three human cancer cell lines: hepatic carcinoma HepG-2, colon carcinoma Caco2, and breast MCF-7 in addition to the normal lung fibroblast WI-38 (Table 1). The obtained results demonstrated that **3**, **4**, **8**, **9a**, and **12d** showed the most potent growth inhibition among all derivatives against the three tested cancer cell lines (Fig. 3). Moreover, derivatives **3** and **4** exhibited more cytotoxic effect than the reference staurosporine against HepG-2 with IC_{50s} 4.57, 0.50 and 13.60 μM, respectively. Furthermore, derivatives **7** and **8** showed substantial cytotoxic activity against HepG-2 with IC_{50s} 19.60 and 11.30 μM, respectively. Similarly, both **4** and **8** revealed better inhibition against Caco2 than staurosporine showing IC_{50s} of 3.19, 5.31, and 8.18 μM, respectively. Likewise, the ethyl ester-containing 2,4,5-trisubstituted thiazole **7** showed slightly better Caco2 cytotoxicity than staurosporine, revealing IC_{50} of 7.39 μM. On the other hand, derivative **4** (IC_{50} = 3.52 ± 0.2 μM) was more potent against MCF-7 than staurosporine (IC_{50} = 6.19 ± 0.3 μM) while **3** demonstrated equipotent activity to staurosporine. Furthermore, remarkable MCF-7 growth inhibition was shown by compounds **1**, **6**, and **7** with IC_{50} 14.90, 21.20, and 12.60 μM, respectively.

In the same context, derivatives **9a** and **12d** were more potent than staurosporine against the three tested cancer cell lines. Yet, the open chain thiosemicarbazone **9a** showed the best growth inhibition potential among all the synthesized derivatives demonstrating IC_{50} 0.53, 1.01, 1.12 μM against HepG-2, Caco2, and MCF-7, respectively. Nevertheless, it showed appreciable inhibition of the normal WI-38 giving IC_{50} 18.4 μM. The most intriguing finding was that derivatives **1**, **6**, and **7** were less hazardous to the normal fibroblast cell line than staurosporine, as indicated by their IC_{50} values (Fig. 3). These findings indicated that these compounds could be considered safer than staurosporine. Similarly, IC_{50} of compounds **9c**, **12b**, and **12d** on normal fibroblasts were higher than staurosporine, confirming their safety preferences. The remaining derivatives exhibited weak to moderate inhibitory activity against the three cancer cell lines with IC_{50} range of 34–153 μM.

2.2.2. Structure–activity relationship analysis. Converting the acetyl moiety of the thiadiazole nucleus **1** to thiosemicarbazone **3** greatly improved the cytotoxic effect towards

 © 2023 The Author(s). Published by the Royal Society of Chemistry

Open Access Article. Published on 10 August 2023. Downloaded on 11/6/2025 1:49:10 AM.
This article is licensed under a Creative Commons Attribution-NonCommercial 3.0 Unported Licence.

Table 1 The cytotoxicity evaluation of derivatives **1**, **3–8**, **9a–d**, **12b**, and **12d** as IC_{50} in μM ± SD and their corresponding hCAIX binding energy score

Compound	hCAIX binding energy (kcal mol^{-1})	IC_{50} (μM ± SD)			
		HepG-2	Caco2	MCF-7	WI-38
1	−10.13	59.60 ± 3.40	11.1 ± 0.60	14.90 ± 0.70	91.50 ± 4.70
3	−10.64	4.57 ± 0.30	14.9 ± 0.70	6.38 ± 0.30	44.40 ± 2.30
4	−11.61	0.50 ± 0.04	3.19 ± 0.20	3.52 ± 0.20	21.40 ± 1.10
6	−11.65	32.90 ± 1.90	33.8 ± 1.70	21.20 ± 1.20	110.00 ± 5.70
7	−11.96	19.60 ± 1.10	7.39 ± 0.40	12.60 ± 0.60	42.90 ± 2.20
8	−11.39	11.30 ± 0.60	5.31 ± 0.30	27.20 ± 1.20	22.90 ± 1.20
9a	−11.47	0.53 ± 0.01	1.01 ± 0.10	1.12 ± 0.10	18.40 ± 1.70
9b	−11.21	149.00 ± 8.40	74.80 ± 3.70	73.00 ± 3.30	92.90 ± 4.80
9c	−11.51	37.10 ± 2.10	34.70 ± 1.70	21.10 ± 0.90	28.50 ± 1.50
9d	−11.52	153.00 ± 8.60	98.70 ± 4.90	42.60 ± 1.80	60.70 ± 3.10
12b	−11.13	17.50 ± 1.50	25.50 ± 1.30	15.10 ± 0.70	63.50 ± 3.90
12d	−12.04	4.26 ± 0.20	1.06 ± 0.10	3.79 ± 0.20	46.60 ± 2.40
Staurosporine	NA[a]	13.60 ± 0.80	8.18 ± 0.70	6.19 ± 0.30	25.20 ± 1.30

[a] NA: not available.

HepG-2 by twelve times and 2.5 times against MCF-7 while preserving **1** cytotoxicity against Caco2 (Table 1). Further increment in the molecule hydrophobicity by cyclizing the thiosemicarbazone terminus **3** into a thiazole ring **4–8** would improve the cell permeability and, ultimately, the cytotoxic effect. This was observed upon mono-substituting the cyclized thiazole with a large hydrophobic moiety like phenyl at C_4 to get **4**, which revealed better cytotoxicity against the three tested cell lines. The added phenyl moiety could increase the overall derivative's lipophilicity, enhancing its cellular uptake. This assumption was supported by the decrement of the cytotoxicity when cyclizing the thiosemicarbazone terminus **3** with the relatively polar thiazolidine-4-one **8** against HepG-2 and MCF-7 by approximately three times.

On the other hand, preserving a small hydrophobic group like a methyl substitution at thiazole C_4 with another H-bond

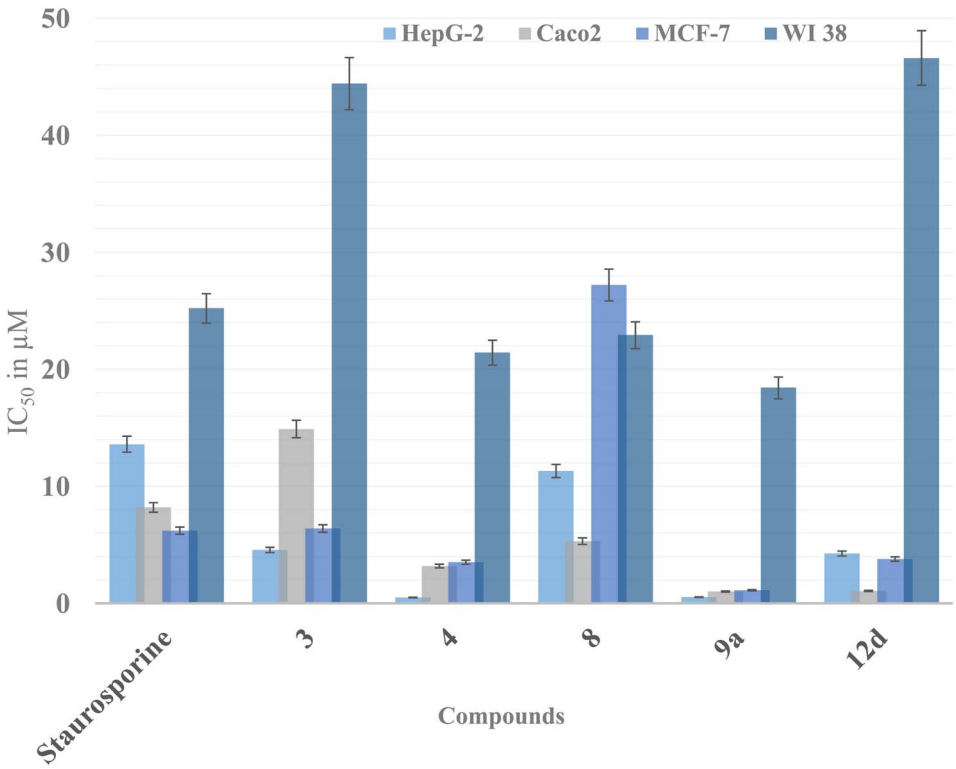

Fig. 3 Graphical presentation of the cytotoxic activity of derivatives **3**, **4**, **8**, **9a** and **12d** against staurosporine as the positive control expressed as IC_{50} (μM).

Open Access Article. Published on 10 August 2023. Downloaded on 11/6/2025 1:49:10 AM.
This article is licensed under a Creative Commons Attribution-NonCommercial 3.0 Unported Licence.

forming moieties like ketone **6** or ester **7** at C_5 did not add much to their cytotoxicity. As concluded, the di-substitution of the thiazole at C_4 and C_5 was not preferable but rather mono-substitution with a phenyl moiety at C_4.

Nevertheless, N3 and C_4 di-substitution of the thiazole ring was evaluated in series **12a–d**. It was observed that incorporating the *para*-chlorophenyl group to N3 with another phenyl ring at C_4 significantly improved the lipophilicity of **12d** compared to the aliphatic allyl substitution at N3 of **12b**. This modification led to 4–25 times improvement of cytotoxicity of **12d** over **12b** against the three tested cell lines, which might be due to the lipophilicity improvement to increase the drug's cellular permeability, as discussed earlier.

In the same context, increasing the lipophilicity of **3** was implemented by another strategy through adding lipophilic moieties such as methyl, allyl, and phenyl groups to the open chain thiosemicarbazone giving derivatives **9a–d**. In this case, the best cytotoxic activity was achieved with the small methyl group substitution at **9a**, showing three to nine times improvement against the three cell lines. Nonetheless, increasing the lipophilic moiety size by adding a phenyl group to the thiosemicarbazone terminus **9c** showed drop-in cytotoxicity by 10 times. Further reduction in the cytotoxicity was observed upon substituting the thiosemicarbazone terminus with an allyl or *para*-chlorophenyl group of **9b** and **9d**, respectively. The size of the added substitution to the thiosemicarbazone terminus of **3** reduced the cytotoxicity probably by interfering with the possible interactions of the terminal sulfur of **3** with the active site residues of hCAIX, as discussed later in the molecular docking simulation (Fig. 5a). A summary of the effect of the structural modification of **3** on the activity is illustrated in Fig. 4.

2.2.3. *In silico* molecular docking simulation. Molecular docking simulations of derivatives **1**, **3–8**, **9a–d**, and **12a–d** were conducted using hCAIX (PDB 3IAI, 2.20 Å) as a possible target to rationalize the obtained cytotoxic result.[30] The protein crystal was prepared as mentioned in the methodology section then the docking protocol was validated before starting the docking simulation. The validation included re-docking the co-crystallized **AAZ** to the binding site using different algorithms until getting the best binding orientation retaining the interaction pattern with the lowest RMSD. The validated molecular docking algorithm of hCAIX showed RMSD 0.374 Å (ESI, Fig. S59†).

The achieved molecular docking results (Tables 1 and 2, Fig. 5–7 and S60 and S61†) revealed better binding energy scores of all the tested benzenesulfonamide derivatives than **AAZ** ranging from −10.13 to −12.04 kcal mol^{-1} compared to −8.83 kcal mol^{-1} of **AAZ**. Moreover, all derivatives conserved the usual zinc coordination between the deprotonated nitrogen and one of the oxygen groups of the sulfonamide moiety (Table 2). It is well established that the sulfonamide nitrogen gets deprotonated in the physiological pH unveiling a negative charge that anchors the zinc ion.[31,32] The zinc ion is an essential cofactor in maintaining the catalytic activity of the hCA isoforms.[7,10,33] Therefore interfering with it would ultimately hinder hCA activity. The bi-dentate coordination of the derivatives sulfonamide moiety to zinc ion would replace the bound water/hydroxide ion from the zinc at the enzyme's active site as an establishing mechanism to initiate the catalytic inhibition.[11,34]

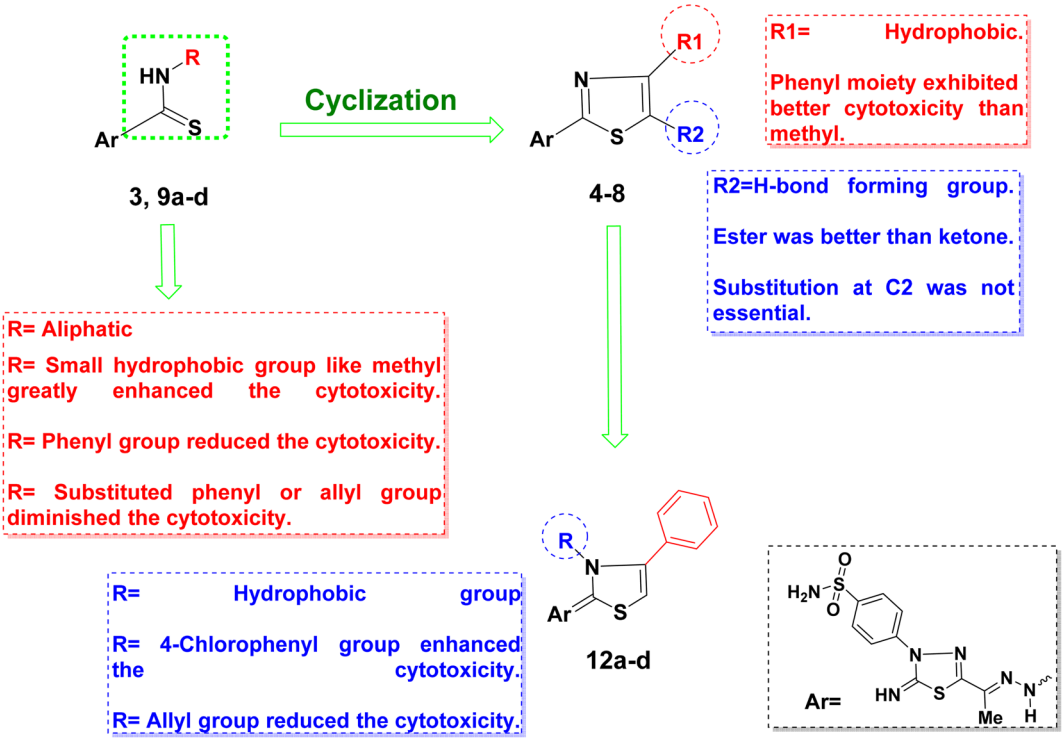

Fig. 4 Schematic representation of the structure–activity relationship of the synthesized derivatives.

 © 2023 The Author(s). Published by the Royal Society of Chemistry

Open Access Article. Published on 10 August 2023. Downloaded on 11/6/2025 1:49:10 AM.
This article is licensed under a Creative Commons Attribution-NonCommercial 3.0 Unported Licence.

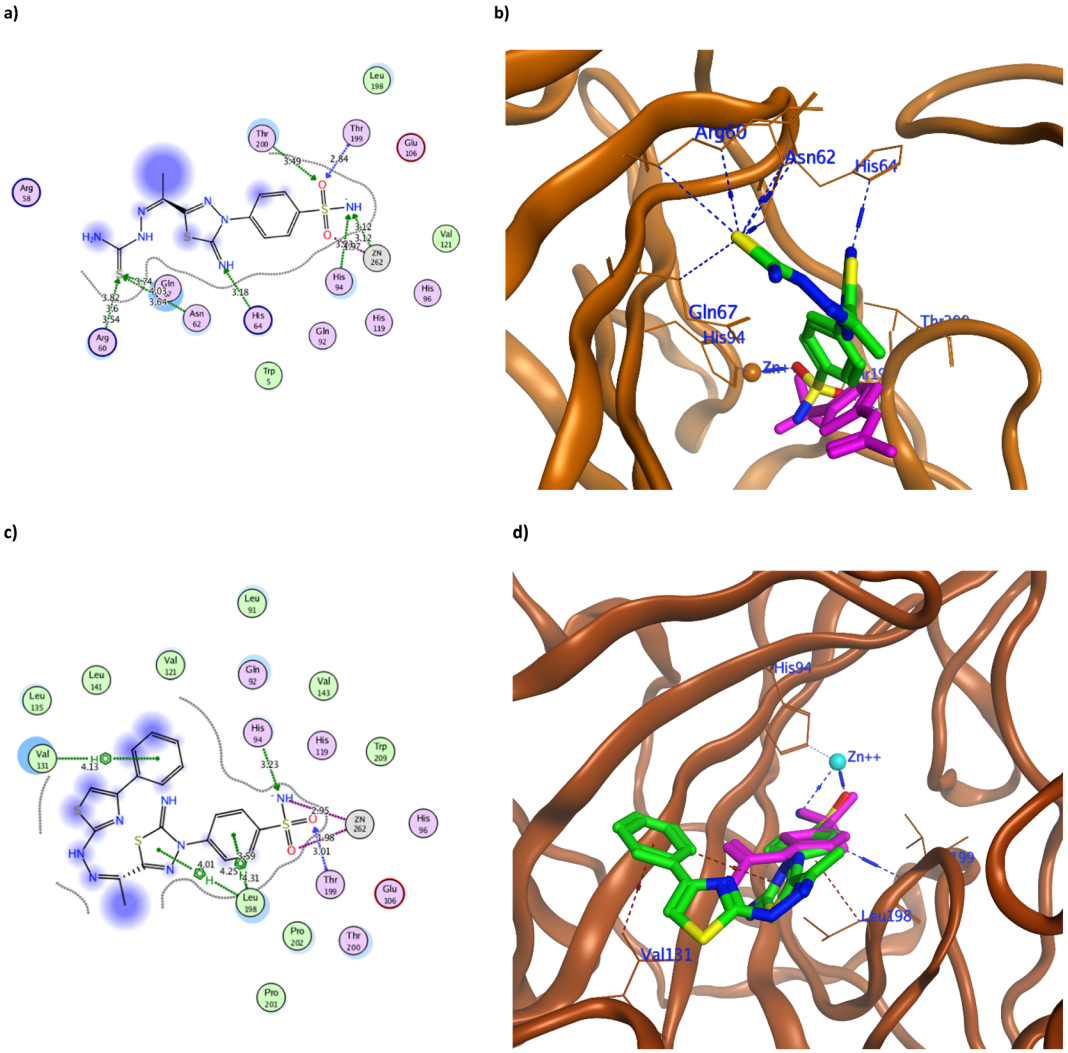

Fig. 5 The 2D and 3D binding pattern of molecular docking simulation of **3** (a and b) and **4** (c and d) using hCAIX (PDB 3IAI, 2.20 Å). The tested derivatives were shown in the stick model in green relative to **AAZ** in magenta color, with the H-bonds and hydrophobic interaction appearing in blue and red dotted lines, respectively.

Moreover, all tested derivatives maintained the H-bond formation with the active site Thr199, similar to **AAZ**. Additionally, the most potent derivatives **3**, **4**, **8**, **9a**, **9c**, and **12d** managed to form H-bond with one of the hCAIX catalytic histidine triad His94 with an average distance of 3.30 Å that augmented with their biological activity (Fig. 5–7).[10]

It was observed that replacing the terminal acetyl moiety of **1** with thiourea in **3** allowed the derivative to interact with Gln67, Asn62, and Arg60 through H-bonds. In addition, it adopted a conformation that allowed the deprotonated nitrogen of **3** to approach His94 and Thr200, thus enhancing its cytotoxicity against HepG-2 and MCF-7 (Fig. 5a and b and S60a†). Conversely, cyclizing the terminal thiourea into a thiazole ring with phenyl group **4** preserved the H-bond with Thr199 and the catalytic His94 with extra hydrophobic interaction with Val131 (Fig. 5c and d). However, replacing the terminal phenyl moiety of **4** with an acetyl group, **6**, greatly decreased its cytotoxic effect by losing the interaction with His94 and Val131 (Fig. S60c†). Changing the acetyl group with an ethyl ester **7** achieved a proper conformation to interact with His64, Leu135, Thr199, Leu198, and Pro201 (Fig. 6a) that was translated into double the cytotoxic effect on HepG-2 and MCF-7. Unlike the small molecule **AAZ**, this extended thiazole ring with ethyl ester of **7** adopted a conformation that filled the unoccupied active site region with the interaction with residues His64 and Pro201 (Fig. 6b). Similarly, altering the ester group with a carbonyl moiety **8** maintained the interaction with His64, and Gln67 at the unoccupied pocket of the active site (Fig. 6c and d). Moreover, it demonstrated further improvement in the cytotoxicity by regaining the H-bond with His94 and additional H-bond with the active site His64 (Fig. 6c). The role of His64 in shuttling the proton during hCAs catalytic activity was valued, especially with its proven inward and outward conformation.[13]

Among the aliphatic substituted thiourea derivatives **9a–d**, derivatives **9a** and **9c** exhibited the best binding conformation inside hCAIX active site while maintaining the H-bond with

Open Access Article. Published on 10 August 2023. Downloaded on 11/6/2025 1:49:10 AM.
This article is licensed under a Creative Commons Attribution-NonCommercial 3.0 Unported Licence.

Table 2 The molecular docking simulation results of derivatives **1**, **3–8**, **9a–d**, and **12a–d** using hCAIX (PDB 3IAI, 2.20 Å)

	Ligand		hCAIX (PDB: 3IAI)			Interaction		
Compound	Interacting moiety		Interacting moiety	Interacting residue		Interaction type	Distance (Å)	Energy (kcal mol^{-1})
AAZ	N3	11	OG1	Thr	200	H-acceptor	3.04	−0.90
	O1	14	N	Thr	199	H-acceptor	2.98	−4.40
	O3	16	NE2	Gln	92	H-acceptor	3.07	−0.70
	N1	8	ZN	Zn	262	Ionic	2.03	−15.60
	O2	15	ZN	Zn	262	Ionic	3.15	−3.50
	5-ring		CD2	Leu	198	Pi-H	3.76	−0.70
1	O	17	N	Thr	199	H-acceptor	2.97	−4.70
	N	16	ZN	Zn	262	Ionic	2.68	−7.00
	O	18	ZN	Zn	262	Ionic	2.00	−16.20
	6-ring		CD2	Leu	198	Pi-H	3.87	−0.20
3	N	4	ND1	His	64	H-acceptor	3.18	−4.80
	S	13	CB	Arg	60	H-acceptor	3.82	−0.70
	S	13	CD	Arg	60	H-acceptor	3.60	−1.00
	S	13	NH1	Arg	60	H-acceptor	3.54	−2.50
	S	13	CB	Asn	62	H-acceptor	4.03	−0.80
	S	13	ND2	Asn	62	H-acceptor	3.64	−3.90
	S	13	CB	Gln	67	H-acceptor	3.74	−0.70
	O	21	N	Thr	199	H-acceptor	2.84	−3.00
	O	21	OG1	Thr	200	H-acceptor	3.49	−0.50
	N	23	CE1	His	94	H-acceptor	3.23	−0.30
	O	22	ZN	Zn	262	Ionic	1.97	−16.80
	N	23	ZN	Zn	262	Ionic	3.12	−3.70
4	N	23	CE1	His	94	H-acceptor	3.23	−0.30
	O	24	N	Thr	199	H-acceptor	3.01	−4.50
	N	23	ZN	Zn	262	Ionic	2.95	−4.80
	O	25	ZN	Zn	262	Ionic	1.98	−16.60
	6-ring		CG2	Val	131	Pi-H	4.13	−0.60
	6-ring		CB	Leu	198	Pi-H	4.31	−0.50
	5-ring		CD1	Leu	198	Pi-H	4.01	−0.30
	6-ring		CD1	Leu	198	Pi-H	4.25	−0.40
	6-ring		CD2	Leu	198	Pi-H	3.59	−0.40
5	O	23	N	Thr	199	H-acceptor	3.02	−4.40
	N	22	ZN	Zn	262	Ionic	2.02	−15.90
	O	24	ZN	Zn	262	Ionic	3.03	−4.20
	6-ring		CD2	Leu	198	Pi-H	4.26	−0.40
6	O	17	ND1	His	64	H-acceptor	2.85	−3.90
	O	26	N	Thr	199	H-acceptor	2.92	−4.90
	N	24	ZN	Zn	262	Ionic	2.08	−14.70
	O	25	ZN	Zn	262	Ionic	2.78	−6.20
	6-ring		CD2	Leu	198	Pi-H	3.54	−0.40
7	N	10	O	Pro	201	H-donor	2.98	−1.50
	S	12	O	Pro	201	H-donor	3.63	−2.90
	O	17	ND1	His	64	H-acceptor	2.98	−2.60
	O	25	N	Thr	199	H-acceptor	2.90	−5.00
	N	24	ZN	Zn	262	Ionic	2.69	−6.90
	O	26	ZN	Zn	262	Ionic	1.97	−16.70
	5-ring		CD2	Leu	135	Pi-H	4.87	−0.70
	6-ring		CD2	Leu	198	Pi-H	3.59	−0.60
8	S	12	OE1	Gln	67	H-donor	3.23	−1.80
	N	8	ND1	His	64	H-acceptor	3.38	−2.60
	O	16	CB	His	64	H-acceptor	3.36	−0.20
	N	23	CA	Leu	198	H-acceptor	3.43	−0.90
	N	23	N	Thr	199	H-acceptor	3.33	−5.90
	O	25	CE1	His	94	H-acceptor	3.38	−0.20
	O	24	ZN	Zn	262	Ionic	1.93	−17.70
	O	25	ZN	Zn	262	Ionic	3.43	−2.20
	6-ring		CD2	Leu	198	Pi-H	4.55	−0.20
9a	N	14	NE2	Gln	92	H-acceptor	3.38	2.80
	O	23	CE1	His	94	H-acceptor	3.47	−0.30
	O	24	CA	Leu	198	H-acceptor	3.18	−0.40

 © 2023 The Author(s). Published by the Royal Society of Chemistry

Open Access Article. Published on 10 August 2023. Downloaded on 11/6/2025 1:49:10 AM.
This article is licensed under a Creative Commons Attribution-NonCommercial 3.0 Unported Licence.

Table 2 (*Contd.*)

Compound	Ligand		hCAIX (PDB: 3IAI)			Interaction		
	Interacting moiety		Interacting moiety	Interacting residue		Interaction type	Distance (Å)	Energy (kcal mol^{-1})
	O	24	N	Thr	199	H-acceptor	3.03	−4.00
	N	22	ZN	Zn	262	Ionic	2.00	−16.30
9b	N	7	NE2	Gln	92	H-acceptor	3.50	−0.70
	O	23	N	Thr	199	H-acceptor	2.96	−4.80
	N	22	ZN	Zn	262	Ionic	2.67	−7.10
	O	24	ZN	Zn	262	Ionic	1.98	−16.60
9c	N	22	CE1	His	94	H-acceptor	3.28	−0.80
	O	23	N	Thr	199	H-acceptor	3.05	−4.00
	N	22	ZN	Zn	262	Ionic	3.35	−2.50
	O	24	ZN	Zn	262	Ionic	1.94	−17.40
	5-ring		CZ2	Trp	5	Pi-H	4.34	−0.50
	6-ring		CG1	Val	131	Pi-H	3.60	−0.40
9d	O	24	N	Thr	199	H-acceptor	2.92	−4.90
	N	22	ZN	Zn	262	Ionic	2.08	−14.80
	O	23	ZN	Zn	262	Ionic	2.59	−7.90
	6-ring		CB	Asp	132	Pi-H	3.74	−0.80
12a	O	25	N	Thr	199	H-acceptor	2.88	−5.10
	N	24	ZN	Zn	262	Ionic	2.48	−9.10
	O	26	ZN	Zn	262	Ionic	1.93	−17.60
12b	O	25	ZN	Zn	262	H-acceptor	2.92	−0.40
	O	26	N	Thr	199	H-acceptor	2.96	−4.70
	N	24	ZN	Zn	262	Ionic	2.06	−15.10
	O	25	ZN	Zn	262	Ionic	2.92	−5.00
	6-ring		CG2	Val	131	Pi-H	4.22	−0.50
	5-ring		CD1	Leu	198	Pi-H	4.12	−0.30
	6-ring		CD2	Leu	198	Pi-H	3.54	−0.30
12c	O	25	N	Thr	199	H-acceptor	2.95	−4.80
	N	24	ZN	Zn	262	Ionic	2.68	−7.00
	O	26	ZN	Zn	262	Ionic	1.97	−16.70
	6-ring		CD2	Leu	198	Pi-H	4.24	−0.30
12d	N	53	CE1	His	94	H-acceptor	3.33	−0.60
	O	56	CA	Leu	198	H-acceptor	3.27	−0.30
	O	56	N	Thr	199	H-acceptor	3.07	−3.90
	N	53	ZN	Zn	262	Ionic	3.34	−2.60
	O	55	ZN	Zn	262	Ionic	1.93	−17.60
	6-ring		CD2	Leu	91	Pi-H	4.81	−0.20
	6-ring		NE2	Gln	92	Pi-H	4.55	−0.80
	6-ring		CG1	Val	131	Pi-H	4.61	−0.30
	6-ring		CG2	Val	131	Pi-H	4.27	−0.30

His94 by their sulfonamide moiety (Fig. 7a and b and S60e†). Moreover, **9a** showed other H-bonds with Gln92, Leu198, and Thr199 with an average distance of 3.20 Å (Fig. 7a). In a similar way; among the cyclized thiazole derivatives **12a–d**, derivative **12d** was the best oriented inside hCAIX with the lowest binding energy of −12.04 kcal mol^{-1}. The deprotonated nitrogen of **12d** conserved the H-bond with His94, while the terminal *para* chloro-substituted phenyl displayed additional hydrophobic interactions with Gln92 and Val131 (Fig. 7c and d). Furthermore, **12d** showed multiple interactions with hCAIX active site residues Leu198, Thr199, and Leu91 that rationalized its good cytotoxicity.

Acknowledging the similarity between the CA isoenzymes, molecular docking simulation was performed using hCAI, hCAII, and hCAXII for the most potent derivatives **4**, **9a**, and **12d** to assess their off-target potentials. Their molecular docking simulation used the reported PDB: 3W6H,[35] 3HS4,[36] and 1JD0 (ref. 37) for hCAI, hCAII, and hCAXII, respectively. The attained data revealed the unfavorable binding pattern of the tested derivatives to the evaluated isoenzymes in contrast to hCAIX (Table 3 and ESI, Fig. S62–S64†). The deprotonated sulfonamide moiety of the three derivatives exhibited the classical coordination with zinc among the evaluated isoenzymes similar to hCAIX. Although **4** and **9a** demonstrated H-bond formation with Thr199, this solely formed bond was not expected to be sufficient for appreciable enzyme inhibition. Moreover, **12d** is only bound to Thr199 in the case of hCAII, not the other isoenzymes and showed single coordination with zinc of 3.27 Å length. In the same context, the predicted binding conformation and interaction of these promising derivatives with the

Open Access Article. Published on 10 August 2023. Downloaded on 11/6/2025 1:49:10 AM.
This article is licensed under a Creative Commons Attribution-NonCommercial 3.0 Unported Licence.

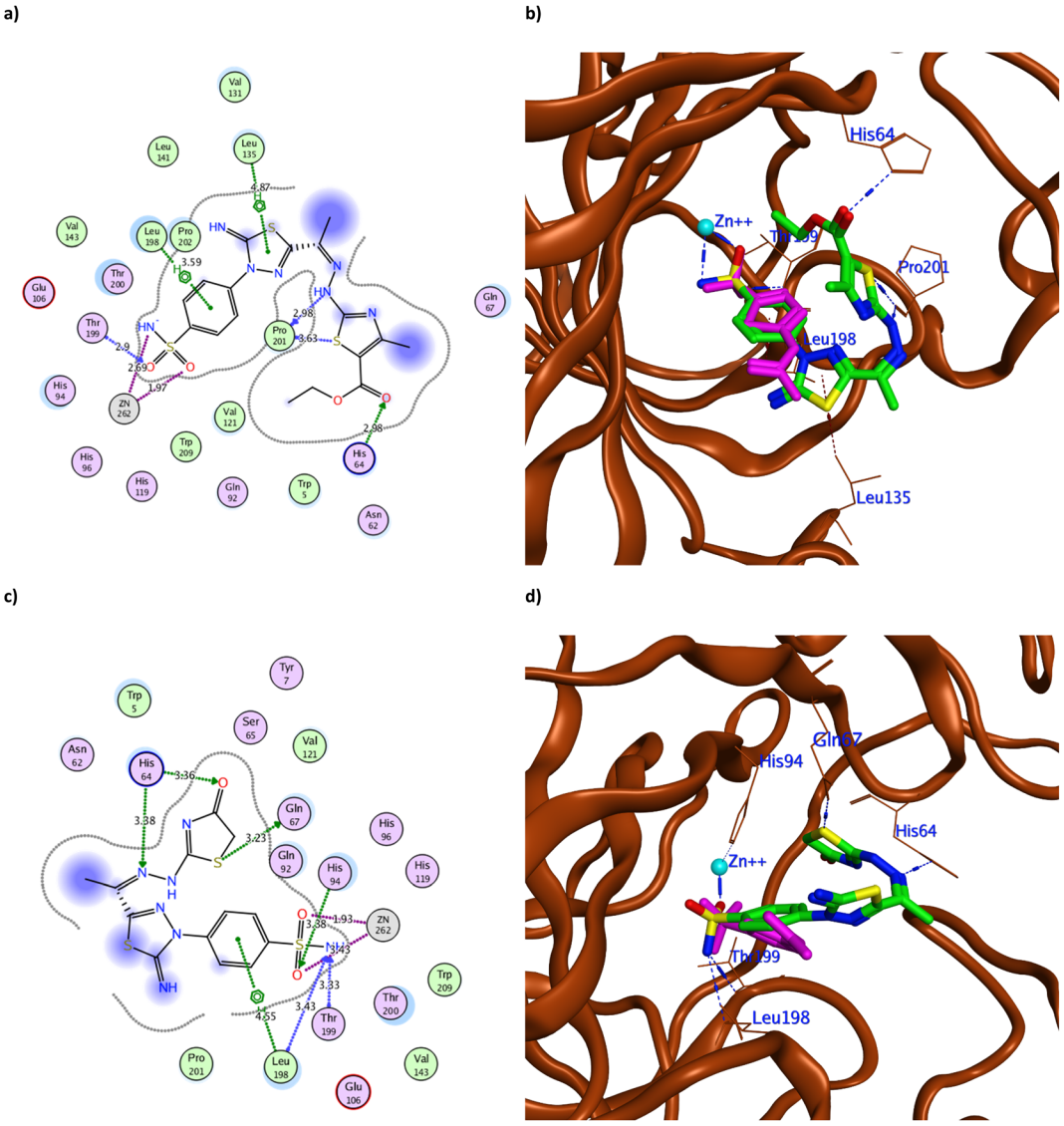

Fig. 6 The 2D binding pattern of molecular docking simulation of **7** (a and b) and **8** (c and d) using hCAIX (PDB 3IAI, 2.20 Å) showing distance in Å. The tested derivatives were shown in the stick model in green relative to **AAZ** in magenta color, with the H-bonds and hydrophobic interaction appearing in blue and red dotted lines, respectively.

tumor-associated hCAXII supported the assumption of exerting their anticancer activity through hCAIX inhibition, not hCAXII.

2.2.4. Molecular dynamics simulation of 9a and 9d. To further verify the suggested hCAIX mechanism for the obtained anticancer activity, the most potent derivative, **9a**, was submitted for molecular dynamic simulation against its least potent congener, **9d**, to test their hCAIX binding complex's stability. Their docked poses were validated using 100 ns-long molecular dynamics (MD) simulation where **9a** demonstrated good stability inside the hCAIX binding site (PDB code: 3IAI) across the simulation (Fig. 8a). Moreover, its simulation revealed RMSD of 1.95 Å demonstrating stable H-bonds (~3 H-bonds on average) throughout MD simulation (Fig. 8b). In contrast, **9d** was less stable exhibiting higher RMSD fluctuation with average 4.1 Å (Fig. 8a) which established from 1 to 2 H-bonds on average showing highly fluctuating H-bond pattern (Fig. 8c).

Accordingly, the overall interaction energies of both derivatives averaged around −61.07 and −22.58 kcal mol^{-1}, respectively (Fig. 9). Furthermore, their calculated binding free energies ($\Delta G_{binding}$) in terms of MM-PBSA were found to be −9.6 and −4.3 kcal mol^{-1}, respectively showing a significant difference in affinities between the two structures towards the active site of hCAIX (Table 4). Accordingly, **9a** was likely more active as an inhibitor of hCAIX in comparison to **9d**.

2.2.5. Physicochemical, pharmacokinetics properties and drug-likeness prediction. The promising derivatives **3**, **4**, **7**, **8**, **9a**, **12b**, and **12d** were *in silico* evaluated in terms of their physicochemical, pharmacokinetics, and drug-likeness using the SwissADME® interface (Table 5).[38] Despite their structural

 © 2023 The Author(s). Published by the Royal Society of Chemistry

Open Access Article. Published on 10 August 2023. Downloaded on 11/6/2025 1:49:10 AM.
This article is licensed under a Creative Commons Attribution-NonCommercial 3.0 Unported Licence.

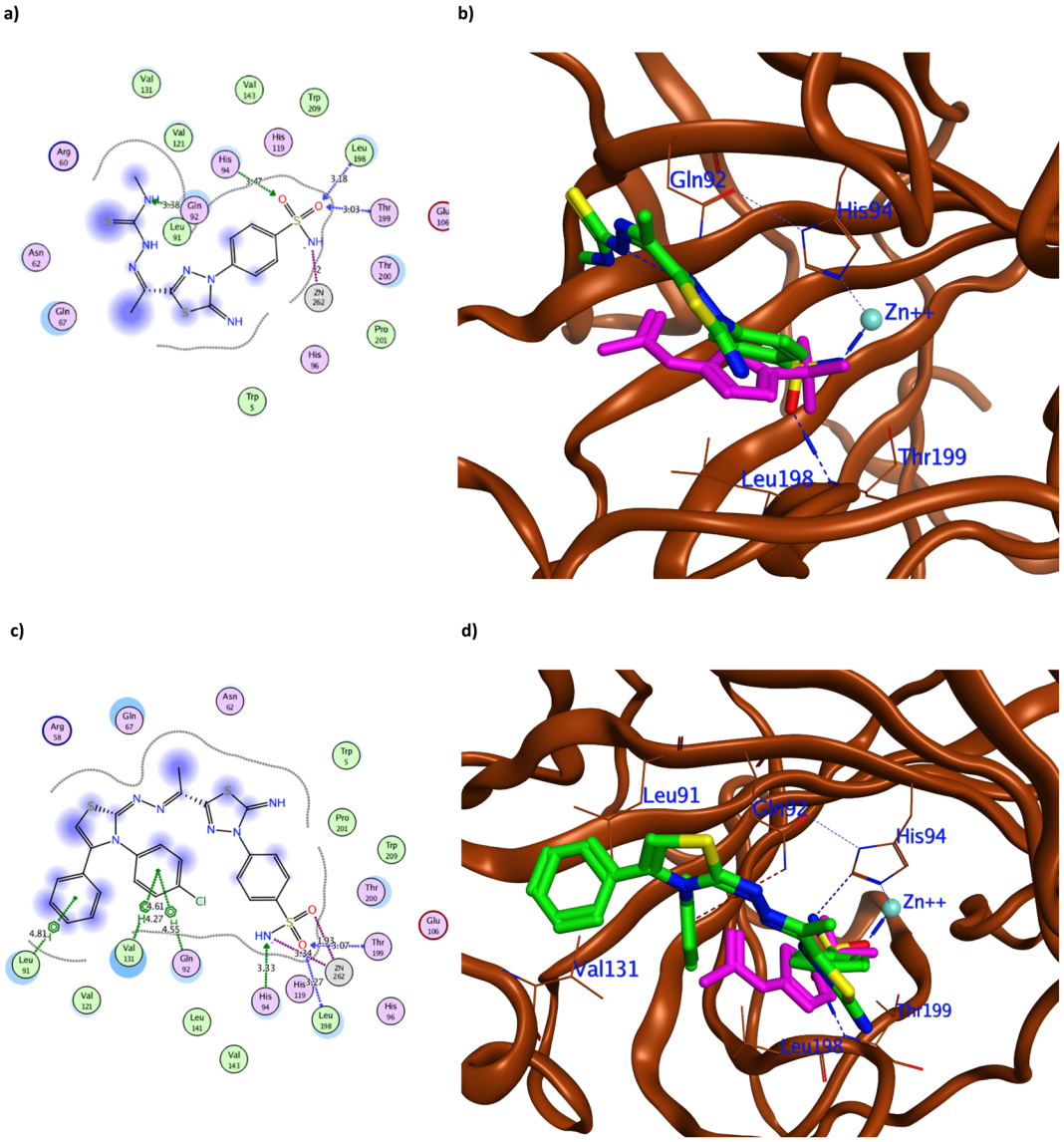

Fig. 7 The 2D and 3D binding pattern of molecular docking simulation of **9a** (a and b) and **12d** (c and d) using hCAIX (PDB 3IAI, 2.20 Å). The tested derivatives were shown in the stick model in green relative to **AAZ** in magenta color, with the H-bonds and hydrophobic interaction appearing in blue and red dotted lines, respectively.

differences, derivatives **9a**, **12b** and **12d** shared the same lipophilicity values. As expected from their chemical structures, all evaluated derivatives showed high polarity and were moderately soluble in an aqueous medium. This polarity was demonstrated in their topological polar surface area TPSA that exceeded 140 Å,[38,39] which was beneficial for their low CNS permeation, and negligible binding to the efflux P-glycoprotein.[40] The low lipophilic characters of the tested derivatives did not affect the liver cytochrome P-450 isoenzymes. Nonetheless, it negatively affected GI absorption and skin permeation, requiring better lipophilic characteristics.

On the other hand, all tested derivatives had acceptable drug-likeness properties according to Lipinski's rule, with one violation of molecular weight of more than 500 g mol^{-1} for **12b** and **12d**.[41,42] However, their bioavailability scores revealed good physiological activity according to Abbott's bioavailability score.[43]

3. Experimental section

3.1. Synthesis and spectroscopic characterization

3.1.1. Synthesis of 2-(1-(5-imino-4-(4-sulfamoylphenyl)-4,5-dihydro-1,3,4-thiadiazol-2-yl)ethylidene)hydrazine-1-carbothioamide (3). A mixture of **1** (2.22 g, 0.007 mol) and thiosemicarbazide **2a** (0.67 g, 0.007 mol) in EtOH (30 ml), concentrated HCl (0.15 ml), was refluxed for 4 h. Compound **3** was obtained by filtering the precipitate, washing it with EtOH, drying it, and recrystallizing it from EtOH. Orange powder; yield 76%; mp > 300 °C; IR ν_{max}/cm^{-1} = 3434, 3340, 3244, 3151 (2NH$_2$), 3141, 3102 (2NH), 1640 (C=N), 1596 (C=C), 1335, 1282

Open Access Article. Published on 10 August 2023. Downloaded on 11/6/2025 1:49:10 AM.
This article is licensed under a Creative Commons Attribution-NonCommercial 3.0 Unported Licence.

Table 3 The molecular docking simulation results of **4**, **9a** and **12d** using hCAI, hCAII and hCAXII

Compound	hCAI (PDB: 3W6H)				hCAII (PDB: 3HS4)				hCAXII (PDB: 1JD0)			
	Binding energy (kcal mol^{-1})	Interacting residue	Interaction type	Distance (Å)	Binding energy (kcal mol^{-1})	Interacting residue	Interaction type	Distance (Å)	Binding energy (kcal mol^{-1})	Interacting residue	Interaction type	Distance (Å)
4	−10.24	Thr 199	H-acceptor	3.21	−10.59	Thr 199	H-acceptor	2.96	−11.53	Thr 199	H-acceptor	3.01
		Zn 302	Ionic	2.03		Zn 301	Ionic	2.76		Zn 901	Ionic	2.82
		Zn 302	Ionic	2.68		Zn 301	Ionic	2.05		Zn 901	Ionic	1.95
9a	−11.13	Asn 69	H-acceptor	3.53	−10.35	Thr 199	H-acceptor	3.10	−10.93	Lys 67	H-acceptor	3.35
		Thr 199	H-acceptor	2.93		Zn 301	Ionic	2.03		Thr 199	H-acceptor	3.01
		Zn 302	Ionic	2.01		Zn 301	Ionic	3.02		Zn 901	Ionic	2.85
		Zn 302	Ionic	3.10						Zn 901	Ionic	1.95
12d	−7.43	Gln 92	H-acceptor	3.56	−7.35	Thr 199	H-acceptor	2.95	−8.42	Zn 262	Ionic	3.27
		Zn 262	Ionic	3.23		Zn 262	Ionic	2.67				
		Val 131	Pi-H	4.14		Zn 262	Ionic	1.99				
						Val 131	Pi-H	4.21				

(SO_2), 1248 (C=S); ^{1}H-NMR (DMSO-d$_6$): δ_{ppm} = 2.32 (s, 3H, CH_3), 7.39 (s, 2H, NH_2), 7.64 (s, 1H, ^{4}N–H$_b$), 7.87 (d, J = 8.5 Hz, 2H, Ar–H$_{2,6}$), 8.23 (d, J = 8.5 Hz, 2H, Ar–H$_{3,5}$), 8.60 (s, 1H, ^{4}N–H$_a$), 9.41 (s, 1H, C=NH), 10.83 (s, 1H, NH); ^{13}C-NMR (DMSO-d$_6$): δ_{ppm} = 12.50 (CH_3), 121.52 (2CH Ar–C$_{2,6}$), 126.45 (2CH Ar–C$_{3,5}$), 140.26 (Ar–C$_4$), 141.38 (Ar–C$_1$), 141.94 (C=N), 148.62 (thiadiazole-C$_2$), 158.56 (thiadiazole-C$_5$), 179.07 (C=S); MS m/z (%): 371 (M$^+$, 1.3), 370 (1.9), 367 (1.8), 366 (2.0), 356 (1.7), 339 (2.1), 326 (1.3), 312 (1.6), 297 (5.1), 285 (2.3), 281 (1.7), 273 (1.5), 258 (1.6), 172 (1.5), 93 (12.7), 83 (58.1), 57 (100). Anal. calc. For $C_{11}H_{13}N_7O_2S_3$ (371.45): C, 35.57; H, 3.53; N, 26.40%; found: C, 35.56; H, 3.54; N, 26.41%.

3.1.2. General procedure for the preparation of thiazole derivatives (4–8). To a solution of **3** (0.8 g, 0.002 mol) in EtOH (30 ml) containing AcONa (1 g, 0.01 mol) and DMF (5 mL), α-chlorocarbonyl compounds (0.002 mol) was added. The reaction mixture was heated under reflux for 3–6 h, then cooled before being put into ice-cold water (50 ml). The precipitate was filtered and recrystallized from EtOH to yield the desired compounds **4–8**.

*3.1.2.1. 4-(2-Imino-5-(1-(2-(4-phenylthiazol-2-yl)hydrazineylidene)ethyl)-1,3,4-thiadiazol-3(2H)yl)benzenesulfonamide (**4**).* The compound was obtained by heating 2-bromo-1-phenylethan-1-one (0.42 g, 0.002 mol) for 3 h under reflux. Brown powder; yield 84%; mp 279–281 °C; IR ν_{max}/cm^{-1} = 3305, 3237 (NH_2), 3197, 3109 (2NH), 1657 (C=N), 1548 (C=C), 1328, 1267 (SO_2); ^{1}H-NMR (DMSO-d$_6$): δ_{ppm} = 2.33 (s, 3H, CH_3), 7.49 (s, 2H, NH_2), 7.55 (s, 1H, thiazole-C$_5$), 7.32–8.22 (m, 9H, Ar–H), 9.45 (s, 1H, NH), 12.05 (s, 1H, NH); ^{13}C-NMR (DMSO-d$_6$): δ_{ppm} = 12.86 (CH_3), 106.82 (thiazole-C$_5$), 121.80 (2CHAr–C$_{2,6}$), 126.01 (2CHAr–C$_{2',6'}$), 126.45 (1CHAr–C$_{4'}$), 126.99 (2CHAr–C$_{3',5'}$), 127.32 (2CHAr–C$_{3,5}$), 128.28 (Ar–C$_4$), 129.19 (Ar–C$_{1'}$), 140.30 (Ar–C$_1$), 142.54 (C=N), 152.82 (thiadiazole-C$_5$), 158.83 (thiazole-C$_4$), 162.82 (thiadiazole-C$_2$), 168.83 (thiazole-C$_2$); MS m/z (%): 471 (M$^+$, 15.6), 470 (0.7), 464 (0.2), 456 (0.4), 392 (2.4), 382 (0.3), 356 (0.6), 259 (1.0), 217 (0.7), 191 (0.9), 176 (9.6), 134 (100), 92 (1.1), 66 (7.7), 54 (6.1). Anal. calc. For $C_{19}H_{17}N_7O_2S_3$ (471.57): C, 48.39; H, 3.63; N, 20.79%; found: C, 48.38; H, 3.64; N, 20.78%.

*3.1.2.2. 4-(2-Imino-5-(1-(2-(4-methylthiazol-2-yl)hydrazineylidene)ethyl)-1,3,4-thiadiazol-3(2H)-yl)benzenesulfonamide (**5**).* The compound was obtained by heating 1-chloropropan-2-one (0.19 g, 0.002 mol) for 7 h under reflux. Brown powder; yield 94%; mp 259–260 °C; IR ν_{max}/cm^{-1} = 3291, 3186 (NH_2), 3142, 3101 (NH), 1602 (C=N), 1558 (C=C), 1320, 1304 (SO_2); ^{1}H-NMR (DMSO-d$_6$): δ_{ppm} = 2.13 (s, 3H, CH_3), 2.26 (s, 3H, CH_3), 6.30 (s, 1H, thiazole-C$_2$), 7.37 (s, 2H, NH_2), 7.87 (d, J = 8.5 Hz, 2H, Ar–H$_{2,6}$), 8.24 (d, J = 8.5 Hz, 2H, Ar–H$_{3,5}$), 9.29 (s, 1H, NH), 11.79 (s, 1H, NH); ^{13}C-NMR (DMSO-d$_6$): δ_{ppm} = 13.34 (CH_3), 17.46 (CH_3), 106.82 (thiazole-C$_5$), 121.21 (2CHAr–C$_{2,6}$), 127.42 (2CHAr–C$_{3,5}$), 129.29 (Ar–C$_4$), 140.01.42 (Ar–C$_1$), 142.09 (C=N), 149.77 (thiazole-C$_4$), 158.89 (thiadiazole-C$_5$), 162.82 (thiadiazole-C$_2$), 168.83 (thiazole-C$_2$); MS m/z (%): 409 (M$^+$, 4.4), 367 (3.0), 313 (4.3), 299 (1.9), 269 (2.1), 262 (1.6), 207 (4.5), 199 (1,6), 177 (2.4), 153 (8.8), 117 (9.0), 99 (23.9), 76 (71.7), 65 (62.7), 59 (100), 51 (20.5); anal. calc. For $C_{14}H_{15}N_7O_2S_3$ (409.50): C, 41.06; H, 3.69; N, 23.94%; found: C, 41.05; H, 3.68; N, 23.93%.

 © 2023 The Author(s). Published by the Royal Society of Chemistry

Open Access Article. Published on 10 August 2023. Downloaded on 11/6/2025 1:49:10 AM.
This article is licensed under a Creative Commons Attribution-NonCommercial 3.0 Unported Licence.

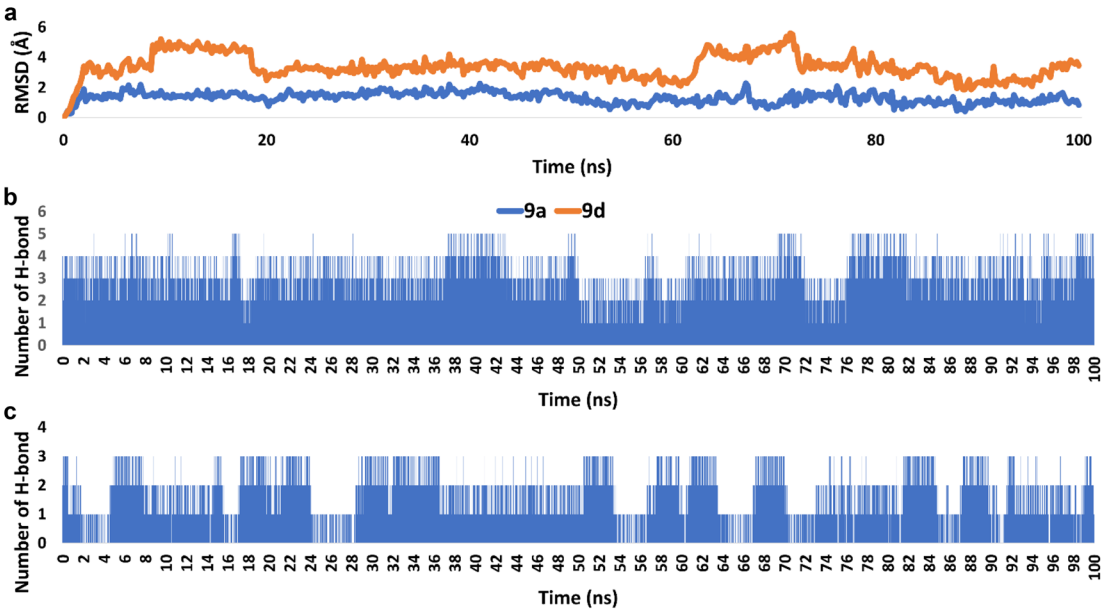

Fig. 8 (a) RMSDs of derivatives **9a** and **9d** inside the active site of hCAIX (PDB ID: 3IAI) throughout 100 ns-long MD simulation. (b) and (c) The number of H-bonds detected for **9a** and **9d**, respectively inside the active site of hCAIX over the course of 100 ns-long MD simulation. The cut-off distance for H-bonds was set to be 2.5 Å.

*3.1.2.3. 4-(5-(1-(2-(5-Acetyl-4-methylthiazol-2-yl) hydrazineylidene)ethyl)-2-imino-1,3,4-thiadi azol-3(2H)-yl)benzenesulfonamide (**6**).* The compound was obtained by heating 3-chloro-2,4-pentanedione (0.29 ml, 0.002 mol) for 5 h under reflux. Brown powder; yield 82%; mp 260–262 °C; IR ν_{max}/cm^{-1} = 3300, 3237 (NH_2), 3197, 3105 (2NH), 1668 (C=O), 1585 (C=N), 1488 (C=C), 1305, 1277 (SO_2); ^{1}H-NMR (DMSO-d$_6$): δ_{ppm} = 2.19 (s, 3H, CH_3), 2.26 (s, 3H, CH_3), 2.39 (s, 3H, CH_3), 7.35 (s, 2H, NH_2), 7.85 (d, J = 8.5 Hz, 2CH, Ar–H$_{2,6}$), 8.22 (d, J = 8.5 Hz, 2CH, Ar–H$_{3,5}$), 9.25 (s, 1H, NH), 11.79 (s, 1H, NH); ^{13}C-NMR (DMSO-d$_6$): δ_{ppm} = 12.98 (CH_3), 27.48 (CH_3), 30.87 (CH_3), 113.48 (2CHAr–C$_{2,6}$), 126.43 (2CHAr–C$_{3,5}$), 126.54 (Ar–C$_4$), 140.05 (thiazole-C$_5$), 141.05 (Ar–C$_1$), 143.25 (C=N), 149.39 (thiadiazole-C$_5$), 158.73 (thiazole-C$_4$), 162.45 (thiadiazole-C$_2$), 169.63 (thiazole-C$_2$), 189.00 (C=O); MS m/z (%): 451 (M$^+$, 32.9), 450 (1.9), 393 (2.9), 326 (1.4), 305 (1.8), 414 (2.1), 296 (1.8), 253 (1.5), 209 (2.1), 171 (5.6), 118 (9.5), 92 (65.1), 77 (27.0), 67 (100), 56 (19.5); anal. calc. For $C_{16}H_{17}N_7O_3S_3$ (451.54): C, 42.56; H, 3.80; N, 21.71%; found: C, 42.55; H, 3.81; N, 21.72%.

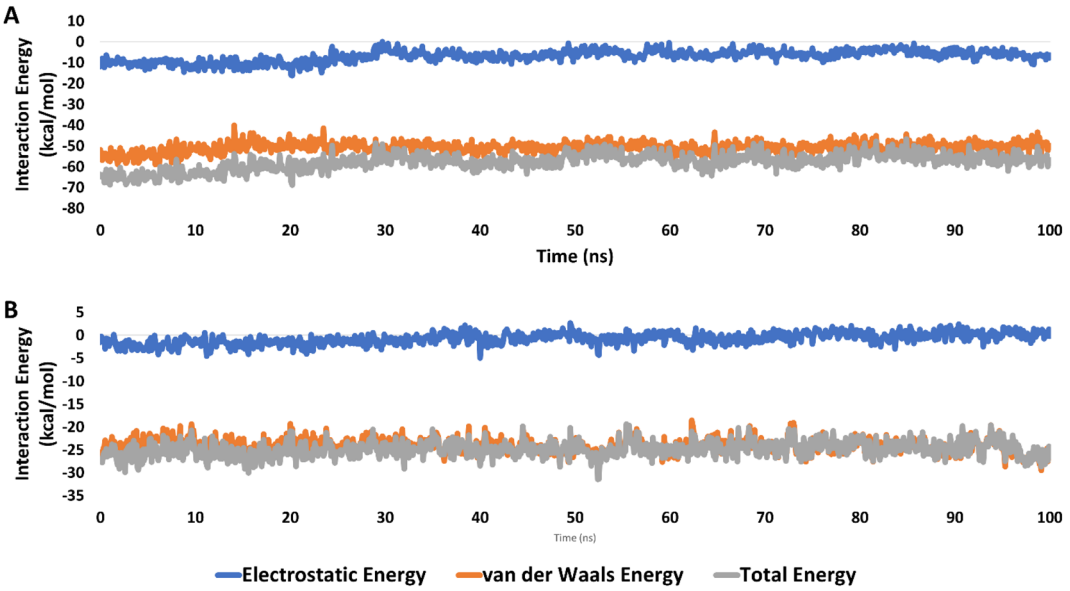

Fig. 9 Interaction energies (*i.e.*, electrostatic and van der Waals interaction energies) of **9a** and **9d** (A and B, respectively) inside the active site of hCAIX (PDB ID: 3IAI) for 100 ns-long MD simulation.

Open Access Article. Published on 10 August 2023. Downloaded on 11/6/2025 1:49:10 AM.
This article is licensed under a Creative Commons Attribution-NonCommercial 3.0 Unported Licence.

Table 4 Binding free energies ($\Delta G_{binding}$) of compounds **9a** and **9d** in complex with the hCAIX (PDB ID: 3IAI) calculated in kcal mol^{-1}

Energy component (kcal mol^{-1})	**9a**	**9d**
ΔG_{gas}	−21.7654	−14.1167
ΔG_{solv}	12.1875	9.8145
ΔG_{total}	−9.5779	−4.3022

3.1.2.4. Ethyl-2-(2-(1-(5-imino-4-(4-sulfamoylphenyl)-4,5-dihydro-1,3,4-thiadiazol-2-yl)ethylidene)hydrazineyl)-4-methylthiazole-5-carboxylate (7). The compound was obtained by heating ethyl 2-chloro-3-oxobutanoate (0.35 ml, 0.002 mol) for 6 h under reflux. Brown powder; yield 80%; mp 100–102 °C; IR ν_{max}/cm^{-1} = 3310, 3232 (NH_2), 3190, 3115 (2NH), 1683 (C=O), 1654 (C=N), 1540 (C=C), 1320, 1268 (SO_2); ^{1}H-NMR (DMSO-d$_6$): δ_{ppm} = 1.23 (t, J = 6.8 Hz, 3H, CH_3), 2.26 (s, 3H, CH_3), 2.87 (s, 3H, CH_3), 4.19 (q, J = 6.8 Hz, 2H, CH_2), 7.40 (s, 2H, NH_2), 7.89 (d, J = 8.5 Hz, 2H, Ar–$H_{2,6}$), 8.15 (d, J = 8.5 Hz, 2H, Ar–$H_{3,5}$), 9.53 (s, 1H, NH), 12.33 (s, 1H, NH–N); ^{13}C-NMR (DMSO-d$_6$): δ_{ppm} = 12.52 (CH_3), 16.31 (CH_3), 30.86 (CH_3), 60.58 (CH_2), 113.48 (2CHAr–$C_{2,6}$), 121.35 (thiazole-C_5), 126.90 (2CHAr–$C_{3,5}$), 127.35 (Ar–C_4), 141.22 (Ar–C_1), 142.15 (C=N), 146.56 (thiadiazole-C_5), 161.5 (thiazole-C_4), 162.45 (thiadiazole-C_2), 168.38 (thiazole-C_2), 173.72 (C=O); MS m/z (%): 481 (M^+, 11.5); MS m/z (%): 481 (M^+, 11.5), 437 (3.3), 401 (0.9), 382 (1.2), 373 (1.1), 302 (0.8), 294 (0.7), 255 (0.9), 222 (1.7), 199 (3.0), 134 (9.9), 127 (5.7), 96 (14.4), 67 (100), 56 (14.2); anal. calc. For $C_{17}H_{19}N_7O_4S_3$ (481.56): C, 42.40; H, 3.98; N, 20.36%; found: C, 4.41; H, 3.97; N, 20.35%.

*3.1.2.5. 4-(2-Imino-5-(1-(2-(4-oxo-4,5-dihydrothiazol-2-yl) hydrazineylidene)ethyl)-1,3,4-thiadi azol-3(2H)-yl)benzenesulfonamide (**8**).* The compound was obtained by heating ethyl 2-chloroacetate (0.26 ml, 0.002 mol) for 4 h under reflux. Orange powder; yield 86%; mp 193–195 °C; IR ν_{max}/cm^{-1} = 3303, 3278 (NH_2), 3189, 3102 (2NH), 1713 (C=O), 1599 (C=N), 1563 (C=C), 1329, 1305 (SO_2); ^{1}H-NMR (DMSO-d$_6$): δ_{ppm} = 2.32 (s, 3H, CH_3), 3.91 (s, 2H, CH_2), 7.38 (s, 2H, NH_2), 7.88 (d, J = 8.5 Hz, 2H, Ar–$H_{2,6}$), 8.22 (d, J = 8.5 Hz, 2H, Ar–$H_{3,5}$), 9.35 (s, 1H, NH), 12.24

Table 5 The calculated physicochemical descriptors, predicted pharmacokinetics properties and drug-likeness of **3**, **4**, **7**, **8**, **9a**, **12b** and **12d** by SwissADME

Compounds	**3**	**4**	**7**	**8**	**9a**	**12b**	**12d**
Physicochemical properties							
Mol. weight in g mol^{-1}	371.5	471.6	481.6	411.5	385.5	511.6	582.1
#Heavy atoms	23	31	31	26	24	34	38
#Aromatic heavy atoms	11	22	16	11	11	22	28
Fraction Csp^3	0.09	0.05	0.24	0.15	0.17	0.09	0.04
#Rotatable bonds	5	6	8	5	6	6	6
#H-bond acceptors	6	7	9	8	6	7	7
#H-bond donors	4	3	3	3	4	2	2
MR	90.5	122.4	118.0	102.3	95.4	135.9	151.0
TPSA (Å^2)	221.0	204.0	230.3	217.6	207.0	196.3	196.3
Lipophilicity							
iLOGP	1.42	2.48	2.59	1.34	1.53	1.53	1.53
XLOGP3	0.40	3.77	3.06	0.98	0.80	0.80	0.80
Water solubility							
ESOL log S	−2.42	−5.27	−4.61	−2.99	−2.68	−2.68	−2.68
ESOL solubility (mg ml^{-1})	1.42×10^0	2.54×10^{-3}	1.19×10^{-2}	4.19×10^{-1}	8.11×10^{-1}	8.11×10^{-1}	8.11×10^{-1}
ESOL class	Soluble	Moderately soluble	Moderately soluble	Soluble	Soluble	Soluble	Soluble
Pharmacokinetics							
GI absorption	Low	Low	Low	Low	Low	Low	Low
BBB permeant	No	No	No	No	No	No	No
P-gp substrate	No	No	No	No	No	No	No
CYP1A2 inhibitor	No	No	No	No	No	No	No
CYP2C19 inhibitor	No	No	No	No	No	No	No
CYP2C9 inhibitor	No	No	No	No	No	No	No
CYP2D6 inhibitor	No	No	No	No	No	No	No
CYP3A4 inhibitor	No	No	Yes	No	No	No	No
Skin permeation log K_p (cm s^{-1})	−8.28	−6.5	−7.06	−8.11	−8.08	−8.08	−8.08
Drug-likeness							
Lipinski #violations	0	0	1	0	0	0	0
Ghose #violations	0	0	1	0	0	0	0
Veber #violations	1	1	1	1	1	1	1
Egan #violations	1	1	1	1	1	1	1
Muegge #violations	1	1	1	1	1	1	1
Bioavailability score	0.55	0.55	0.55	0.55	0.55	0.55	0.55

 © 2023 The Author(s). Published by the Royal Society of Chemistry

Open Access Article. Published on 10 August 2023. Downloaded on 11/6/2025 1:49:10 AM. This article is licensed under a Creative Commons Attribution-NonCommercial 3.0 Unported Licence.

(s, 1H, N–H); ^{13}C-NMR (DMSO-d$_6$): δ_{ppm} = 12.80 (CH$_3$), 33.15 (CH$_2$), 120.79 (2CHAr–C$_{2,6}$), 126.89 (2CHAr–C$_{3,5}$), 141.92 (Ar–C$_4$), 149.17 (Ar–C$_1$), 153.85 (C=N), 155.85 (thiadiazole-C$_5$), 158.49 (thiadiazole-C$_2$), 165.37 (thiazole-C$_2$), 171.77 (C=O); MS *m/z* (%): 411 (M$^+$, 2.9), 410 (2.2), 367 (1.9), 340 (1.8), 313 (7.7), 297 (1.9), 242 (5.6), 208 (2.1), 197 (1.6), 177 (1.7), 153 (3.7), 111 (17.0), 90 (8.3), 77 (11.3), 61 (8.6), 55 (100); anal. calc. For $C_{13}H_{13}N_7O_3S_3$ (411.47): C, 37.95; H, 3.18; N, 23.83%; found: C, 37.94; H, 3.19; N, 23.82%.

3.1.3. General procedure for the preparation of 2-(1-(5-imino-4-(4-sulfamoylphenyl)-4,5-dihydro-1,3,4-thiadiazol-2-yl) ethylidene)hydrazine-1-carbothioamide derivatives (9a–d). A mixture of **1** (1 g, 0.003 mol) and 4-substituted thiosemicarbazides **2a–d** (0.003 mol) in EtOH (30 ml) containing concentrated HCl (0.25 ml) was refluxed for 2–4 h. The formed precipitate was filtered off, washed with ethanol, dried, and recrystallization from EtOH to afford compounds **9a–d**, respectively.

*3.1.3.1. 2-(1-(5-Imino-4-(4-sulfamoylphenyl)-4,5-dihydro-1,3,4-thiadiazol-2-yl)ethylidene)-N-methylhydrazine-1-carbothioamide (**9a**).* The compound was obtained by heating **2a** (0.35 g, 0.003 mol) for 2 h under reflux. Orange powder; yield 78%; mp 251–253 °C; IR ν_{max}/cm^{-1} = 3339, 3301 (NH$_2$), 3199, 3115, 3109 (3NH), 1628 (C=N), 1559 (C=C), 1327, 1292 (SO$_2$), 1217 (CS); ^{1}H-NMR (DMSO-d$_6$): δ_{ppm} = 2.28 (s, 3H, CH$_3$), 3.04 (d, *J* = 5.1 Hz, 3H, NH–CH$_3$), 7.66 (s, 2H, NH$_2$), 7.92 (d, *J* = 8.5 Hz, 2H, Ar–H$_{2,6}$), 8.05 (d, *J* = 8.5 Hz, 2H, Ar–H$_{3,5}$), 8.70 (s, 1H, NH), 11.04 (s, 1H, NH), 11.43 (s, 1H, NH); ^{13}C-NMR (DMSO-d$_6$): δ_{ppm} = 12.78 (CH$_3$), 31.53 (CH$_3$), 127.20 (2CHAr–C$_{2,6}$), 127.55 (2CHAr–C$_{3,5}$), 137.68 (Ar–C$_4$), 139.07 (Ar–C$_1$), 145.91 (C=N), 155.60 (thiadiazole-C$_2$), 167.79 (thiadiazole-C$_5$), 178.67 (C=S); MS *m/z* (%): 385 (M$^+$, 0.1), 384 (0.1), 379 (0.1), 375 (0.1), 372 (0.1), 369 (0.1), 364 (0.1), 352 (0.2), 346 (0.1), 265 (0.7), 259 (0.2), 245 (0.3), 194 (1.2), 165 (1.7), 95 (22.2), 57 (100). Anal. calc. For $C_{12}H_{15}N_7O_2S_3$ (385.48): C, 37.39; H, 3.92; N, 25.44%; found: C, 37.38; H, 3.93; N, 25.45%.

*3.1.3.2. N-Allyl-2-(1-(5-imino-4-(4-sulfamoylphenyl)-4,5-dihydro-1,3,4-thiadiazol-2-yl)ethylid ene)hydrazine-1-carbothioamide (**9b**).* The compound was obtained by heating **2b** (0.44 g, 0.003 mol) for 4 h under reflux. Orange powder; yield 70%; mp 263–265 °C; IR ν_{max}/cm^{-1} = 3303, 3268 (NH$_2$), 3197, 3120, 3100 (3NH), 1630 (C=N), 1555 (C=C), 1313, 1293 (SO$_2$), 1187 (CS); ^{1}H-NMR (DMSO-d$_6$): δ_{ppm} = 2.30 (s, 3H, CH$_3$), 4.24 (t, *J* = 5.9 Hz, 2H, N–CH$_2$), 5.11 (dd, *J* = 8.5, 1.5 Hz, 1H, CH=), 5.16 (dd, *J* = 15.3, 1.5 Hz, 1H, CH=), 5.88 (m, 1H, CH=), 7.64 (s, 2H, NH$_2$), 7.93 (d, *J* = 8.5 Hz, 2H, Ar–H$_{2,6}$), 8.05 (d, *J* = 8.5 Hz, 2H, Ar–H$_{3,5}$), 8.83 (s, 1H, NH), 9.48 (s, 1H, NH), 11.13 (s, 1H, NH); ^{13}C-NMR (DMSO-d$_6$): δ_{ppm} = 12.81 (CH$_3$), 46.19 (CH$_2$), 115.83 (2CHAr–C$_{2,6}$), 127.03 (CH$_2$), 127.52 (2CHAr–C$_{3,5}$), 134.36 (Ar–C$_4$), 137.74 (Ar–C$_1$), 139.34 (CH), 145.80 (C=N), 155.51 (thiadiazole-C$_2$), 167.64 (thiadiazole-C$_5$), 178.33 (C=S); MS *m/z* (%): 411 (M$^+$, 0.7), 410 (1.1), 396 (1.0), 384 (1.1), 369 (1.9), 354 (2.2), 290 (0.7), 264 (4.5), 126 (3.5), 112 (10.4), 100 (3.4), 57 (100); anal. calc. For $C_{14}H_{17}N_7O_2S_3$ (411.52): C, 40.86; H, 4.16; N, 23.83%; found: C, 40.87; H, 4.17; N, 23.82%.

*3.1.3.3. Synthesis of 2-(1-(5-imino-4-(4-sulfamoylphenyl)-4,5-di-hydro-1,3,4-thiadiazol-2-yl)ethylidene)-N-phenylhydrazine-1-carbothioamide (**9c**).* This compound was obtained by heating **2c** (0.56 g, 0.003 mol) for 4 h under reflux. Orange powder; yield 86%; mp 260–261 °C; IR ν_{max}/cm^{-1} = 3295, 3257 (NH$_2$), 3187, 3114, 3102 (3NH), 1625 (C=N), 1554 (C=C), 1318, 1294 (SO$_2$), 1237 (CS); ^{1}H-NMR (DMSO-d$_6$): δ_{ppm} = 2.35 (s, 3H, CH$_3$), 7.24–756 (m, 5H, Ar–H), 7.65 (s, 2H, NH$_2$), 7.94 (d, *J* = 8.5 Hz, 2H, Ar–H$_{2,6}$), 8.06 (d, *J* = 8.5 Hz, 2H, Ar–H$_{3,5}$), 10.49 (s, 1H, NH), 11.11 (s, 1H, NH), 11.48 (s, 1H, NH); ^{13}C-NMR (DMSO-d$_6$): δ_{ppm} = 13.06 (CH$_3$), 121.54 (2CHAr–C$_{2,6}$), 125.34 (2CHAr–C$_{2',6'}$), 125.84 (1CHAr–C$_{4'}$), 127.15 (2CHAr–C$_{3',5'}$), 127.59 (2CHAr–C$_{3,5}$), 128.47 (Ar–C$_4$), 137.73 (Ar–C$_1$), 138.94 (Ar–C$_1$), 140.04 (C=N), 145.91 (thiadiazole-C$_2$), 167.85 (thiadiazole-C$_5$), 177.61 (C=S); MS *m/z* (%): 447 (M$^+$, 0.2), 423 (0.3), 412 (0.2), 400 (0.2), 382 (0.2), 368 (0.2), 208 (0.2), 179 (0.5), 167 (1.1), 152 (1.3), 137 (0.7), 93 (100), 78 (3.9), 66 (40). Anal. calc. For $C_{17}H_{17}N_7O_2S_3$ (447.55): C, 45.62; H, 3.83; N, 21.91%; found: C, 45.61; H, 3.82; N, 21.92%.

*3.1.3.4. N-(4-Chlorophenyl)-2-(1-(5-imino-4-(4-sulfamoylphenyl)-4,5-dihydro-1,3,4-thiadiazol-2-yl)-ethylidene) hydrazine-1-carbothioamide (**9d**).* The compound was obtained by heating **2d** (0.67 g, 0.003 mol) for 3 h under reflux. Orange powder, yield 87%; mp 262–264 °C; IR ν_{max}/cm^{-1} = 3339, 3258 (NH$_2$), 3165, 3130, 3104 (3NH), 1635 (C=N), 1553 (C=C), 1363, 1292 (SO$_2$), 1247 (CS); ^{1}H-NMR (DMSO-d$_6$): δ_{ppm} = 2.37 (s, 3H, CH$_3$), 7.47 (d, *J* = 8.5 Hz, 2H, Ar–H$_{3',5'}$), 7.61 (d, *J* = 8.5 Hz, 2H, Ar–H$_{2',6'}$), 7.67 (s, 2H, NH$_2$), 7.96 (d, *J* = 8.5 Hz, 2H, Ar–H$_{2,6}$), 8.07 (d, *J* = 8.5 Hz, 2H, Ar–H$_{3,5}$), 10.51 (s, 1H, NH), 10.99 (s, 1H, HN), 11.56 (s, 1H, NH); ^{13}C-NMR (DMSO-d$_6$): δ_{ppm} = 13.50 (CH$_3$), 127.59 (2CHAr–C$_{2,6}$), 127.96 (2CHAr–C$_{3',5'}$), 128.78 (2CHAr–C$_{3,5}$), 130.21 (Ar–C$_4$), 138.18 (2CHAr–C$_{2',6'}$), 138.36 (Ar–C$_{4'}$), 140.80 (Ar–C$_{1'}$), 140.99 (Ar–C$_1$), 143.32 (C=N), 146.23 (thiadiazole-C$_2$), 155.76 (thiadiazole-C$_5$), 178.08 (C=S); MS *m/z* (%): 481 (M$^+$, 0.2), 480 (0.3),467 (0.3), 397 (0.3), 381 (0.2), 367 (0.2), 333 (0.2), 325 (0.2), 295 (0.2), 268 (0.2), 264 (0.4), 254 (0.2), 250 (0.5), 239 (0.5), 227 (0.2), 201 (0.2), 199 (0.2), 191 (0.3), 182 (0.2), 171 (1.4), 127 (100), 93 (4.5), 78 (3.03), 66 (8.9). Anal. calc. For $C_{17}H_{16}ClN_7O_2S_3$ (481.99): C, 42.36; H, 3.35; N, 20.34%; found: C, 42.37; H, 3.35; N, 20.33%.

3.1.4. General procedure for the preparation of 4-(2-imino-5-(1-((4-phenylthiazol-2(3*H*)-ylidene)hydrazono)ethyl)-1,3,4-thiadiazol-3(2*H*)-yl)benzenesulfonamide derivatives (12a–d). To a mixture of compound **9a–d** (0.5 g, 0.001 mol) and 2-bromo-1-phenylethan-1-one (0.001 mol) in EtOH (20 ml) containing TEA (0.15 ml) and DMF (5 ml) was refluxed for 3–6 h. The reaction mixture was allowed to cool to RT before being poured into ice water (40 ml). The formed precipitate was filtered off, dried, and recrystallized from EtOH to yield compounds **12a–d**.

*3.1.4.1. 4-(2-Imino-5-(1-((3-methyl-4-phenylthiazol-2(3H)-ylidene)hydrazono)ethyl)-1,3,4-thiadiazol-3(2H)-yl)benzenesulfonamide (**12a**).* Orange powder; yield 77%; mp 231–233 °C; IR ν_{max}/cm^{-1} = 3334, 3245 (NH$_2$), 3172 (NH), 1652 (C=N), 1582 (C=C), 1324, 1297 (SO$_2$); ^{1}H-NMR (DMSO-d$_6$): δ_{ppm} = 2.33 (s, 3H, CH$_3$), 2.5 (s, 3H, NCH$_3$), 6.56 (s, H, thiazole-H$_5$), 7.39 (s, 2H, NH$_2$),7.51 (s, 5H, Ar–H), 7.88 (d, *J* = 8.5 Hz, 2H, Ar–H$_{2,6}$), 8.25 (d, *J* = 8.5 Hz, 2H, Ar–H$_{3,5}$), 9.33 (s, 1H, NH); ^{13}C-NMR (DMSO-d$_6$): δ_{ppm} = 12.50 (CH$_3$), 33.78 (CH$_3$), 101.48 (thiazole-C$_5$), 120.58 (2CHAr–C$_{2,6}$), 126.46 (1CHAr–C$_{4'}$), 128.85 (2CHAr–C$_{2',6'}$), 128.87 (2CHAr–

Open Access Article. Published on 10 August 2023. Downloaded on 11/6/2025 1:49:10 AM. This article is licensed under a Creative Commons Attribution-NonCommercial 3.0 Unported Licence.

$C_{3',5'}$), 129.09 (2CHAr–$C_{3,5}$), 129.41 (Ar–$C_{1'}$), 130.11 (Ar–C_4), 140.14 (Ar–C_1), 142.01 (thiazole-C_4), 146.83 (C=N), 153.00 (thiadiazole-C_5), 159.19 (thiazole-C_2), 171.56 (thiadiazole-C_2); MS *m/z* (%): 485 (M^+, 25.4), 484 (1.1), 443 (0.1), 412 (0.1), 394 (0.1), 325 (0.1), 315 (0.1), 298 (0.1), 256 (12.0), 190 (2.8), 160 (1.2), 102 (100), 72 (4.1); anal. calc. For $C_{20}H_{19}N_7O_2S_3$ (485.60): C, 49.47; H, 3.94; N, 20.19%; found: C, 49.48; H, 3.93; N, 20.18%.

*3.1.4.2. 4-(5-(1-((3-Allyl-4-phenylthiazol-2(3H)-ylidene)hydrazono)ethyl)-2-imino-1,3,4-thiadiazol-3(2H)-yl)benzenesulfonamide (**12b**).* Orange powder; yield 80%; mp 202–204 °C; IR ν_{max}/cm^{-1} = 3303, 3237 (NH_2), 3165 (NH), 1637 (C=N), 1584 (C=C), 1326, 1287 (SO_2); ^{1}H-NMR (DMSO-d_6): δ_{ppm} = 2.27 (s, 3H, CH_3), 4.47 (d, J = 4.2 Hz, 2H, CH_2), 5.12 (dd, J = 91, 1.7 Hz, 1H, CH=), 5.19 (dd, J = 16, 1.7 Hz, 1H, CH=), 5.82 (m, 1H, CH=), 6.62 (s, 1H, thiazole-H_5), 7.46 (s, 2H, NH_2), 7.47–7.49 (m, 5H, Ar–H), 7.96 (d, J = 8.5 Hz, 2H, Ar–$H_{2,6}$), 8.08 (d, J = 8.5 Hz, 2H, Ar–$H_{3,5}$), 9.98 (s, 1H, NH); ^{13}C-NMR (DMSO-d_6): δ_{ppm} = 12.49 (CH_3), 47.95 (N–CH_2), 102.35 (thiazole-C_5), 117.09 (CH_2), 121.19 (2CHAr–$C_{2,6}$), 126.00 (1CHAr–$C_{4'}$), 126.87 (2CHAr–$C_{2',6'}$), 127.00 (2CHAr–$C_{3',5'}$), 128.82 (2CHAr–$C_{3,5}$), 129.00 (Ar–$C_{1'}$), 129.61 (Ar–C_4), 130.04 (Ar–C_1), 132.07 (CH), 140.75 (thiazole-C_4), 146.27 (C=N), 155.51 (thiadiazole-C_5), 159.51 (thiazole-C_2), 171.48 (thiadiazole-C_2); MS *m/z* (%): 511 (M^+, 15.8), 509 (1.6), 497 (1.3), 454 (3.6), 437 (6.7), 419 (2.4), 391 (1.4), 368 (2.1), 277 (2.6), 256 (9.8), 177 (2.4), 134 (100); anal. calc. For $C_{22}H_{21}N_7O_2S_3$ (511.64): C, 51.65; H, 4.14; N, 19.16%; found: C, 51.66; H, 4.15; N, 19.17%.

*3.1.4.3. 4-(5-(1-((3,4-Diphenylthiazol-2(3H)-ylidene)hydrazono)ethyl)-2-imino-1,3,4-thiadiazol-3(2H)-yl)benzenesulfonamide (**12c**).* Green powder; yield 74%; mp 210–214 °C; IR ν_{max}/cm^{-1} = 3330, 3274 (2NH), 3177 (NH), 1653 (C=N), 1586 (C=C), 1325, 1280 (SO_2); ^{1}H-NMR (DMSO-d_6): δ_{ppm} = 2.07 (s, 3H, CH_3), 6.78 (s, 1H, thiazole-H_5), 7.15–7.31 (m, 10H, Ar–H), 7.44 (s, 2H, NH_2), 7.90 (d, J = 9.3 Hz, 2H, Ar–$H_{2,6}$), 7.99 (d, J = 9.3 Hz, 2H, Ar–$H_{3,5}$), 9.68 (s, 1H, NH); ^{13}C-NMR (DMSO-d_6): δ_{ppm} = 12.61 (CH_3), 103.16 (thiazole-C_5), 121.28 (2CHAr–$C_{2,6}$), 126.78 (1CHAr–$C_{4''}$), 126.89 (2CHAr–$C_{2'',6''}$), 127.31 (1CHAr–$C_{4'}$), 128.32 (2CHAr–$C_{2',6'}$), 128.38 (2CHAr–$C_{3',5'}$), 128.48 (2CHAr–$C_{3',5'}$), 128.50 (2CHAr–$C_{3,5}$), 128.68 (Ar–$C_{1'}$), 128.76 (Ar–C_4), 140.25 (Ar–$C_{1''}$), 140.40 (Ar–C_1), 147.79 (C–N), 148.31 (C=N), 152.73 (thiadiazole-C_5), 162.45 (thiazole-C_2), 172.46 (thiadiazole-C_2); MS *m/z* (%): 547 (M^+, 45.4), 546 (1.9), 523 (1.3), 520 (1.6), 488 (2.6), 487 (4.5), 479 (1.5), 468 (1.9), 443 (1.3), 435 (1.4), 407 (1.7), 393 (1.4), 368 (1.9), 252 (4.9), 239 (4.2), 163 (2.4), 107 (10.9), 92 (21.1), 77 (100), 65 (25.0). Anal. calc. For $C_{25}H_{21}N_7O_2S_3$ (547.67): C, 54.83; H, 3.87; N, 17.90%; found: C, 54.82; H, 3.86; N, 17.91%.

*3.1.4.4. 4-(5-(1-((3-(4-Chlorophenyl)-4-phenylthiazol-2(3H)-ylidene)hydrazono)ethyl)-2-imino-1,3,4-thiadiazol-3(2H)-yl)benzenesulfonamide (**12d**).* Dark green powder; yield 84%; mp 227–230 °C; IR ν_{max}/cm^{-1} = 3303, 3276 (NH_2), 3155 (NH), 1654 (C=N), 1584 (C=C), 1306, 1279 (SO_2), 738 (C–Cl); ^{1}H-NMR (DMSO-d_6): δ_{ppm} = 2.12 (s, 3H, CH_3), 6.81 (s, 1H, thiazole-H_5), 7.18 (d, J = 2.5 Hz, 2H, Ar–$H_{2',6'}$), 7.29 (d, J = 4.2 Hz, 2H, Ar–$H_{3',5'}$), 7.34–7.45 (m, 5H, Ar–H), 7.59 (d, J = 8.5 Hz, 2H, Ar–$H_{2,6}$), 7.90 (d, J = 8.5 Hz, 2H, Ar–$H_{3,5}$), 8.19 (s, 2H, NH_2), 9.49 (s, 1H, NH); ^{13}C-NMR (DMSO-d_6): δ_{ppm} = 12.42 (CH_3), 103.67 (thiazole-C_5), 114.33 (2CHAr–$C_{2,6}$), 121.69 (2CHAr–$C_{2'',6''}$), 127.03 (1CHAr–$C_{4''}$), 127.30 (1CHAr–$C_{4'}$), 128.69 (2CHAr–$C_{2',6'}$), 128.91 (2CHAr–$C_{3',5'}$), 129.37 (2CHAr–$C_{3'',5''}$), 130.03 (2CHAr–$C_{3,5}$), 130.54 (Ar–C_4), 130.83 (Ar–$C_{1'}$), 131.12 (Ar–$C_{1''}$), 133.01 (Ar–C_1), 136.43 (thiazole-C_4), 140.25 (C=N), 148.87 (thiadiazole-C_5), 158.73 (thiazole-C_2), 162.45 (thiadiazole-C_2); MS *m/z* (%): 582 (M^+, 22.1) 584 (M^{2+}, 8.1), 581 (28.5), 524 (1.9), 503 (1.6), 488 (1.9), 425 (1.6), 381 (2.6), 355 (2.6), 351 (1.9), 339 (2.1), 315 (1.7), 294 (1.7), 279 (1.8), 2.51 (2.7), 210 (2.4), 155 (4.1), 127 (7.6), 93 (15.2), 71 (52.1), 57 (100). Anal. calc. For $C_{25}H_{20}ClN_7O_2S_3$ (582.11): C, 51.58; H, 3.46; N, 16.84%; found: C, 51.59; H, 3.47; N, 16.85%.

3.2. Biological evaluation

The evaluated human cancer cell lines were cultivated to ensure their presence in the log phase then 3 mL of the cultivation medium was introduced to 96-well microplate. The total cells count in the medium should not exceed 10^6 cells per cm^2 and the medium did not contain phenol or serum. Afterward, an equivalent volume of MTT (M-5655) to 10% of the medium was added and incubated at room temperature for 2–4 hours. The deposited formazan crystals were dissolved in an equivalent MTT solubilizing solution (M-8910) in the culture medium. The intensity of the obtained solution was measured as absorbance at wavelength 570 nm against the blank solution. The blank solution was prepared following the same conditions without cells at every test.[44,45]

3.3. Molecular docking simulation

The protein structure of hCAIX was recovered from the Protein Data Bank using PDB: 3IAI.[46] Its crystal structure was subjected to the preparation step by deleting the unnecessary chains, co-factors, and water molecules while keeping the zinc ion. The Molecular Operating Environment (MOE) software-embedded autocorrection tool was used to check the validity of the chain conformation then hydrogens were added at a cutoff of 15 Å using AMBER10:EHT forcefield. The molecular docking site was adjusted to a radius of 4.5 Å around the co-crystallized ligand. Afterward, the actual docking simulation was implemented using Triangle Matcher, London dG, and GBVI/WSA as the placement, and rescoring functions 1 and 2, respectively. On the other hand, the chemical structures of the derivatives were constructed using ChemAxon Marvin JS, then pasted as smiles to MOE builder, protonated, and energy minimized at the same forcefield before commencing the simulation protocol.

3.4. Molecular dynamic simulation

The simulation was performed using NAMD 3.0.0, applying Charmm-36 as the forcefield. According to the literature,[47,48] Protein systems were built, corrected and prepared using the QwikMD.[48,49] The binding free energy was calculated according to Molecular Mechanics Poisson–Boltzmann Surface Area (MM-PBSA) embedded in the MMPBSA.py module of AMBER18 (ref. 50) using the following equation:

$$\Delta G_{binding} = \Delta G_{complex} - \Delta G_{receptor} - \Delta G_{inhibitor}$$

 © 2023 The Author(s). Published by the Royal Society of Chemistry

Open Access Article. Published on 10 August 2023. Downloaded on 11/6/2025 1:49:10 AM. This article is licensed under a Creative Commons Attribution-NonCommercial 3.0 Unported Licence.

Each equation required calculating multiple energy components, including van der Waals energy, electrostatic energy, internal energy from molecular mechanics, and polar contribution to solvation energy.

4. Conclusion

Herein, the tail approach synthesized a bundle of different hybrids of disubstituted/trisubstituted 1,3-thiazoles with 1,3,4-thiadiazolylbenzenesulfonaminde started with **1**. The best cytotoxicity was observed with **4** and **9a** against HepG-2, Caco2, and MCF-7 compared to staurosporine, with **4** showing a better safety margin as declared from its WI38 IC_{50} 21.4 μM and 18.4 μM, respectively. Similarly, the phenylthiazole trisubstituted analogue **12d** showed good cytotoxicity against the three tested cancer cell lines with higher safety than both **4** and **9a**, as concluded from its WI38 IC_{50} 46.6 μM. Moreover, the molecular modeling simulation of **4**, **9a**, and **12d** against hCAIX revealed the bidentate coordination with zinc and forming H-bond with the catalytic His94, which explained their astonishing cytotoxicity. The molecular dynamic simulation of the more potent **9a** and the least potent **9d** with hCAIX demonstrated appreciable support of the proposed mechanism of their anticancer activity.

Conflicts of interest

There are no conflicts to declare.

Acknowledgements

The authors thank the Deanship of Scientific Research at King Khalid University for funding this work through Small group Research Project under grant number RGP1/152/44.

References

1 J. Liu, S.-Q. Li, J. Wang, N. Li, J. Zhou and H. Chen, *Recent Pat. Anti-Cancer Drug Discovery*, 2022, **18**, 125–132.
2 A. I. Ilovaisky, A. M. Scherbakov, V. M. Merkulova, E. I. Chernoburova, M. A. Shchetinina, O. V. Andreeva, D. I. Salnikova, I. V. Zavarzin and A. O. Terent'ev, *J. Steroid Biochem. Mol. Biol.*, 2023, **228**, 106245.
3 M. Gümüş, M. Yakan and İ. Koca, *Future Med. Chem.*, 2019, **11**, 1979–1998.
4 M. Arshad, A. Alam, A. S. Alshammari, M. B. Alhazza, I. M. Alzimam, Md. A. Alam, G. Mustafa, M. S. Ansari, A. M. D. A. Alotaibi, A. Alotaibi, S. Kumar, S. M. B. Asdaq, M. Imran, P. K. Deb, K. N. Venugopala and S. Jomah, *Molecules*, 2022, **27**, 3994.
5 P. C. Sharma, K. K. Bansal, A. Sharma, D. Sharma and A. Deep, *Eur. J. Med. Chem.*, 2020, **188**, 112016.
6 A. Jain, S. Sharma, A. Vaidya, R. Veerasamy and R. K. Agrawal, *Chem. Biol. Drug Des.*, 2013, **81**, 557–576.
7 C. T. Supuran, *Nat. Rev. Drug Discovery*, 2008, **7**, 168–181.
8 Y. L. Duc, E. Licsandru, D. Vullo, M. Barboiu and C. T. Supuran, *Bioorg. Med. Chem.*, 2017, **25**, 1681–1686.
9 C. T. Supuran, *Expert Opin. Ther. Pat.*, 2018, **28**, 729–740.
10 C. Temperini, A. Scozzafava and C. T. Supuran, *Bioorg. Med. Chem.*, 2010, **20**, 474–478.
11 C. T. Supuran and A. Scozzafava, *Bioorg. Med. Chem.*, 2007, **15**, 4336–4350.
12 F. Cianchi, M. C. Vinci, C. T. Supuran, B. Peruzzi, P. De Giuli, G. Fasolis, G. Perigli, S. Pastorekova, L. Papucci, A. Pini, E. Masini and L. Puccetti, *J. Pharmacol. Exp. Ther.*, 2010, **334**, 710–719.
13 M. Aggarwal, C. G. Boone, B. Kondeti and R. McKenna, *J. Enzyme Inhib. Med. Chem.*, 2012, **28**, 267–277.
14 C. T. Supuran, *Expert Opin. Ther. Pat.*, 2018, **28**, 709–712.
15 C. W. McMonnies, *J. Optom.*, 2017, **10**, 71–78.
16 R. Kumar, A. Kumar, S. Ram, C. T. Supuran, A. Bonardi, P. Gratteri and P. K. Sharma, *Arch. Pharm.*, 2022, **355**, 2100241.
17 S. Kilicaslan, M. Arslan, Z. Ruya, C. Bilen, A. Ergün, N. Gençer and O. Arslan, *J. Enzyme Inhib. Med. Chem.*, 2016, **31**, 1300–1305.
18 A. A. Almehizia, W. M. Eldehna, C. T. Supuran, H. M. Ibrahim, S. Bua, H. A. Abdel-Aziz and S. M. Abou-Seri, *Bioorg. Chem.*, 2019, **87**, 794–802.
19 P. A. Channar, R. D. Alharthy, S. A. Ejaz, A. Saeed and J. Iqbal, *Molecules*, 2022, **27**, 8723.
20 M. Khan, S. A. Halim, R. Csuk, M. N. Islam, M. A. Shehzad, A. Ibrard, F. R. Khan, N. Marraiki, J. Uddin, A. Khan and A. Al-Harrasi, *Curr. Pharm. Des.*, 2022, **28**, 3010–3022.
21 M. Ishaq, P. Taslimi, R. Csuk, S. Khan, R. E. Salmas, M. M. Zangeneh, A. Saeed, A. Zangeneh, P. Taslimi, A. Asari and H. Mohamad, *Bioorg. Chem.*, 2020, **100**, 103924.
22 A. W. Erian, S. S. Sherif and H. M. Gaber, *Molecules*, 2003, **8**, 793–865.
23 R. Venkatraman, H. Ameera, L. Sitole, E. D. Ellis, F. R. Fronczek and E. J. Valente, *J. Chem. Crystallogr.*, 2009, **39**, 711–718.
24 A. A. Hassan, S. K. Mohamed, N. K. Mohamed, K. M. El-Shaieb, A. T. Abdel-Aziz, J. T. Mague and M. Akkurt, *J. Sulfur Chem.*, 2016, **37**, 162–175.
25 H. Yakan, *Res. Chem. Intermed.*, 2020, **46**, 3979–3995.
26 M. A. Fouad, M. Y. Zaki, R. A. Lotfy and W. H. Mahmoud, *Bioorg. Chem.*, 2021, **112**, 104985.
27 V. V. Syakaev, S. N. Podyachev, B. I. Buzykin, S. K. Latypov, W. D. Habicher and A. I. Konovalov, *J. Mol. Struct.*, 2006, **788**, 55–62.
28 D. T. G. Gonzaga, F. De C Da Silva, V. F. Ferreira, J. L. Wardell and S. M. S. V. Wardell, *J. Braz. Chem. Soc.*, 2016, **27**, 2322–2333.
29 E. Abdel-Latif, M. M. Fahad, A. El-Demerdash and M. A. Ismail, *J. Heterocycl. Chem.*, 2020, **57**, 3071–3081.
30 V. Alterio, M. Hilvo, A. Di Fiore, C. T. Supuran, P. Pan, S. Parkkila, A. Scaloni, J. Pastorek, S. Pastorekova, C. Pedone, A. Scozzafava, S. M. Monti and G. De Simone, *Proc. Natl. Acad. Sci.*, 2009, **106**, 16233–16238.
31 K. Kanamori and J. D. Roberts, *Biochemistry*, 1983, **22**, 2658–2664.
32 N. Chiaramonte, M. N. Romanelli, E. Teodori and C. T. Supuran, *Metabolites*, 2018, **8**, 36.
33 C. T. Supuran, *Expert Opin. Invest. Drugs*, 2018, **27**, 963–970.

Open Access Article. Published on 10 August 2023. Downloaded on 11/6/2025 1:49:10 AM.
This article is licensed under a Creative Commons Attribution-NonCommercial 3.0 Unported Licence.

34 S. Imran, M. Taha, N. H. Ismail, S. Fayyaz, K. M. Khan and M. I. Choudhary, *Bioorg. Chem.*, 2015, **62**, 83–93.
35 Y. Takaoka, Y. Kioi, A. Morito, J. Otani, K. Arita, E. Ashihara, M. Ariyoshi, H. Tochio, M. Shirakawa and I. Hamachi, *Chem. Commun.*, 2013, **49**, 2801–2803.
36 K. H. Sippel, A. H. Robbins, J. F. Domsic, C. Genis, M. Agbandje-McKenna and R. McKenna, *Acta Crystallogr., Sect. A: Found. Crystallogr.*, 2009, **65**, 992–995.
37 D. A. Whittington, A. Waheed, B. Ulmasov, G. N. Shah, J. H. Grubb, W. S. Sly and D. W. Christianson, *Proc. Natl. Acad. Sci.*, 2001, **98**, 9545–9550.
38 A. Daina, O. Michielin and V. Zoete, *Sci. Rep.*, 2017, **7**, 42717.
39 A. T. Balaban, *Theor. Chim. Acta*, 1979, **53**, 355–375.
40 J. Lin and M. Yamazaki, *Clin. Pharmacokinet.*, 2003, **42**, 59–98.
41 C. A. Lipinski, *Drug Discovery Today: Technol.*, 2004, **1**, 337–341.
42 C. A. Lipinski, F. Lombardo, B. W. Dominy and P. W. Feeney, *Adv. Drug Delivery Rev.*, 1997, **23**, 3–25.
43 Y. C. Martin, *J. Med. Chem.*, 2005, **48**, 3164–3170.
44 S. Bondock, T. Albarqi, T. Nasr, N. M. Mohamed and M. M. Abdou, *Arabian J. Chem.*, 2023, **16**, 104956.
45 S. Bondock, T. Albarqi, I. A. Shaaban and M. M. Abdou, *RSC Adv.*, 2023, **13**, 10353–10366.
46 F. Briganti, S. Mangani, P. Orioli, A. Scozzafava, G. Vernaglione and C. T. Supuran, *Biochemistry*, 1997, **36**, 10384–10392.
47 J. G. Phillips, R. Braun, W. Wang, J. C. Gumbart, E. Tajkhorshid, E. Villa, C. Chipot, R. D. Skeel, L. V. Kale and K. Schulten, *J. Comput. Chem.*, 2005, **26**, 1781–1802.
48 J. Ribeiro, R. C. Bernardi, T. Rudack, K. Schulten and E. Tajkhorshid, *Biophys. J.*, 2018, **114**, 673a–674a.
49 W. Humphrey, A. Dalke and K. Schulten, *J. Mol. Graphics*, 1996, **14**, 33–38.
50 B. R. Miller, T. D. McGee, J. M. Swails, N. Homeyer, H. Gohlke and A. E. Roitberg, *J. Chem. Theory Comput.*, 2012, **8**, 3314–3321.

 © 2023 The Author(s). Published by the Royal Society of Chemistry